CERN-TH/2001-308
JINR E2–2000–292
`hep-ph/0012080`
revised version
November 2001

An electroweak library for the calculation of EWRC to $e^+e^- \to f\bar{f}$ within the CalcPHEP project

D. Bardin, L. Kalinovskaya, and G. Nanava

Laboratory for Nuclear Problems, JINR, ul. Joliot-Curie 6,

RU-141980 Dubna, Russia

Abstract

We present a description of calculations of the electroweak amplitude for $e^+e^- \to t\bar{t}$ process. The calculations are done within the OMS (on-mass-shell) renormalization scheme in two gauges: in R_ξ, which allows an explicit control of gauge invariance by examining cancellation of gauge parameters and search for gauge-invariant subsets of diagrams, and in the unitary gauge as a cross-check. The formulae we derived are realized in a FORTRAN code eeffLib, which is being created within the framework of the project CalcPHEP. We present a comprehensive comparison between eeffLib results for the light top with corresponding results of the well-known program ZFITTER for the $u\bar{u}$ channel, as well as a preliminary comparison with results existing in the world literature.

CERN-TH/2001–308
November 2001

Work supported in part by INTAS N^o 00-00313.

E-mails: bardin@nusun.jinr.ru, kalinov@nusun.jinr.ru, nanava@nusun.jinr.ru

Contents

List of Figures

List of Tables

Introduction

The process $e^+e^- \to t\bar{t}$ has already been studied for about ten years in connection with experiments at future linear colliders (see, for instance, the review [1]).

Actually, it is a six-fermion process (see [2]); one of the channels is shown in Fig. 1.

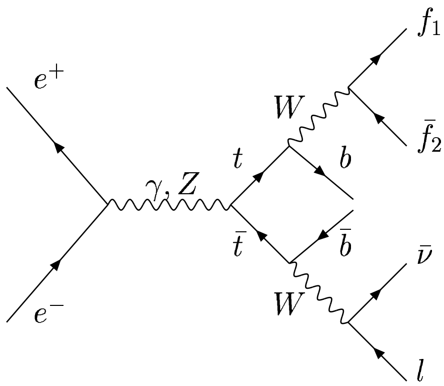

Figure 1: The six-fermion $e^+e^- \to t\bar{t}$ process.

However, the cross-section of a hard subprocess, $\sigma(e^+e^- \to t\bar{t})$, with tops on the mass shell is an ingredient in various approaches, such as DPA [3] or the so-called Modified Perturbation Theory (MPT), see [4].

In this article, we present a brief description of a calculation of the electroweak part of the *amplitude* of the $e^+e^- \to t\bar{t}$ process. This calculation is a part of the project `CalcPHEP` [5] which started in Y2K after completion of the well-known project `ZFITTER` [6]. One of main goals of this paper is to cross-check the `CalcPHEP` results against the results obtained with the other existing codes.

As before, we use the OMS renormalization scheme, a complete presentation of which was recently made in [7]. However, for the first time we performed calculations in two gauges: R_ξ and the unitary gauge.

Note that there was wide experience of calculations in the R_ξ gauge for processes such as $H \to f\bar{f}, WW, ZZ, \gamma Z, \gamma\gamma$, or $e^+e^- \to ZH, WW$. So, in [8] and [9] a complete set of one-loop counterterms for the SM is given. Electromagnetic form factors for arbitrary ξ are discussed in [10] and [11]. Explicit expressions can be found in the CERN library program EEWW [12].

However, we are not aware of the existence of calculations in the R_ξ gauge for the $e^+e^- \to t\bar{t}$ process, although there are many studies in the $\xi = 1$ gauge, see [13] – [16].

Additional purposes of this study are:

– to explicitly control gauge invariance in R_ξ by examining cancellation of gauge parameters, and search for gauge-invariant subsets of diagrams;

– to offer a possibility to compare the results with those in the unitary gauge, as a cross-check;

– to present a self-contained list of results for one-loop amplitude in terms of Passarino–Veltman functions A_0, B_0, C_0 and D_0 and their combinations in the spirit of the book [7], where the process $e^+e^- \to t\bar{t}$ was not covered; this article may thus be considered as an Annex to this book;

– to create a `FORTRAN` code for the calculation of the improved Born approximation (IBA) amplitudes and of the electroweak (EW) part of the cross-section of this process for a complementary study within the MPT framework;

This article consists of five sections.

In Section 1, we present the Born amplitude of the process, basically to introduce our notation and then define *the basis* in which the one-loop amplitude was calculated. We explain *the splitting* between QED and EW corrections and between 'dressed' γ and Z exchanges.

Section 2 contains explicit expressions for all *the building blocks*: self-energies, vertices and EW boxes. Note that no diagram was computed by hand. They are supplied by a new system, `CalcPHEP`, which is being created at the site `brg.jinr.ru`. It roots back to dozens of supporting `form` codes written by authors of [7] while working on it. Later on, the idea came up to collect, order, unify and upgrade these codes up to the level of a 'computer system'. Its first phase will be described elsewhere [5].

In Section 3, we describe the procedure of construction of *the scalar form factors* of the one-loop amplitudes out of the building blocks. One of the aims of this section is to create a frame for a subsequent realization of this procedure within the `CalcPHEP` project.

Section 4 contains explicit expressions for the IBA cross-section.

Finally, in Section 5 we present results of a comprehensive numerical comparison between `eeffLib` and `ZFITTER`. We also discuss some preliminary results of a comparison between `eeffLib` and the other available codes.

1 Amplitudes

1.1 Born amplitudes

We begin with the Born amplitudes for the process $e^+(p_+)e^-(p_-) \to t(q_-)\bar{t}(q_+)$, which is described by the two Feynman diagrams with γ and Z exchange. The Born amplitudes are:

$$
\begin{aligned}
A^{B}_{\gamma} &= eQ_e\, eQ_t \gamma_\mu \otimes \gamma_\mu \frac{-i}{Q^2} = -i\, 4\pi\alpha(0) \frac{Q_e Q_t}{Q^2} \gamma_\mu \otimes \gamma_\mu \,, && (1.1)\\
A^{B}_{Z} &= \frac{e}{2s_W c_W} \frac{e}{2s_W c_W} \gamma_\mu \left[I^{(3)}_e \gamma_+ - 2Q_e s^2_W \right] \otimes \gamma_\mu \left[I^{(3)}_t \gamma_+ - 2Q_t s^2_W \right] \frac{-i}{Q^2+M^2_Z} \\
&= -ie^2 \frac{1}{4s^2_W c^2_W (Q^2+M^2_Z)} \Bigl[I^{(3)}_e I^{(3)}_t \gamma_\mu\gamma_+ \otimes \gamma_\mu\gamma_+ + \delta_e I^{(3)}_t \gamma_\mu \otimes \gamma_\mu\gamma_+ \\
&\quad + I^{(3)}_e \delta_t \gamma_\mu\gamma_+ \otimes \gamma_\mu + \delta_e\delta_t \gamma_\mu \otimes \gamma_\mu \Bigr] \,, && (1.2)
\end{aligned}
$$

where $\gamma_\pm = 1 \pm \gamma_5$ and the symbol $\otimes$ is used in the following short-hand notation:

$$
\gamma_\mu \left(L_1\gamma_+ + Q_1\right) \otimes \gamma_\nu \left(L_2\gamma_+ + Q_2\right) = \bar{v}\left(p_+\right) \gamma_\mu \left(L_1\gamma_+ + Q_1\right) u\left(p_-\right) \bar{u}\left(q_-\right) \gamma_\nu \left(L_2\gamma_+ + Q_2\right) v\left(q_+\right); \qquad (1.3)
$$

furthermore

$$
\delta_f = v_f - a_f = -2Q_f s^2_W \,, \qquad f = e, t. \qquad (1.4)
$$

Introducing the LL, QL, LQ, and QQ structures, correspondingly (see last Eq. (1.2)), we have five structures to which the complete Born amplitude may be reduced: one for the γ exchange amplitude and four for the Z exchange amplitude.

1.2 One-loop amplitude for $e^+e^- \to t\bar{t}$

For the $e^+e^- \to t\bar{t}$ process at one loop, it is possible to consider a gauge-invariant subset of *electromagnetic corrections* separately: QED vertices, $\gamma\gamma$ and $Z\gamma$ boxes. Together with QED bremsstrahlung diagrams, it is free of infrared divergences. The contribution of QED diagrams is considered elsewhere [17]. Here we keep in mind only the remaining one-loop diagrams forming *electroweak corrections*. The total electroweak amplitude is a sum of 'dressed' γ and Z exchange amplitudes, plus the contribution from *the weak box* diagrams (WW and ZZ boxes).

Contrary to the Born amplitude, the one-loop amplitude may be parametrized by 6 form factors, a number equal to the number of independent helicity amplitudes for this process.

We work in the so-called LQD basis, which naturally arises if the final-state fermion masses are not ignored [1]. Then the amplitude may be schematically represented as:

$$
\left[i\gamma_\mu\gamma_+ F^e_L(s) + i\gamma_\mu F^e_Q(s) \right] \otimes \left[i\gamma_\mu\gamma_+ F^t_L(s) + i\gamma_\mu F^t_Q(s) + m_t I D_\mu F^t_D(s) \right], \qquad (1.5)
$$

[1] If the initial-state masses were not ignored too, we would have ten independent helicity amplitudes, ten structures and ten scalar form factors.

with

$$D_\mu = (q_+ - q_-)_\mu \,. \tag{1.6}$$

Every form factor in the R_ξ gauge could be represented as a sum of two terms:

$$F^{\xi}_{L,Q,D}(s) = F^{(1)}_{L,Q,D}(s) + F^{\rm add}_{L,Q,D}(s)\,. \tag{1.7}$$

The first term corresponds to the $\xi = 1$ gauge and the second contains all ξ dependences and vanishes for $\xi = 1$ by construction.

The LQD basis was found to be particularly convenient to explicitly demonstrate the cancellation of all ξ-dependent terms. We checked the cancellation of these terms in several groups of diagrams separately: the so-called γ, Z, and H clusters, defined below; the W cluster together with the self-energies and the WW box; and the ZZ boxes. Therefore, for our process we found seven separately gauge-invariant subgroups of diagrams: three in the QED sector, and four in the EW sector.

The 'dressed' γ exchange amplitude is

$$A^{\rm IBA}_{\gamma} = i\frac{4\pi Q_e Q_f}{s}\alpha(s)\gamma_\mu \otimes \gamma_\mu\,, \tag{1.8}$$

which is identical to the Born amplitude of Eq. (1.2) modulo the replacement of $\alpha(0)$ by the running electromagnetic coupling $\alpha(s)$:

$$\alpha(s) = \frac{\alpha}{1-\dfrac{\alpha}{4\pi}\left[\Pi^{\rm fer}_{\gamma\gamma}(s) - \Pi^{\rm fer}_{\gamma\gamma}(0)\right]}\,. \tag{1.9}$$

In the LQD basis the Z exchange amplitude has the following Born-like structure in terms of six (LL, QL, LQ, QQ, LD and QD) form factors:

$$\begin{aligned}
\mathcal{A}^{\rm IBA}_{Z} \;=\;& i\,e^2\frac{\chi_Z(s)}{s}\Bigl\{\gamma_\mu\gamma_+ \otimes \gamma_\mu\gamma_+ \tilde{F}_{LL}(s,t) + \gamma_\mu \otimes \gamma_\mu\gamma_+ \tilde{F}_{QL}(s,t)\\
&+\gamma_\mu\gamma_+ \otimes \gamma_\mu \tilde{F}_{LQ}(s,t) + \gamma_\mu \otimes \gamma_\mu \tilde{F}_{QQ}(s,t)\\
&+\gamma_\mu\gamma_+ \otimes \left(-im_t D_\mu\right)\tilde{F}_{LD}(s,t) + \gamma_\mu \otimes \left(-im_t D_\mu\right)\tilde{F}_{QD}(s,t)\Bigr\},
\end{aligned} \tag{1.10}$$

where we introduce the notation for $\tilde{F}_{ij}(s,t)$:

$$\begin{aligned}
\tilde{F}_{LL}(s,t) &= I^{(3)}_e I^{(3)}_t F_{LL}(s,t)\,,\\
\tilde{F}_{QL}(s,t) &= \delta_e I^{(3)}_t F_{QL}(s,t)\,,\\
\tilde{F}_{LQ}(s,t) &= I^{(3)}_e \delta_t F_{LQ}(s,t)\,,\\
\tilde{F}_{QQ}(s,t) &= \delta_e \delta_t F_{QQ}(s,t)\,,\\
\tilde{F}_{LD}(s,t) &= I^{(3)}_e I^{(3)}_t F_{LD}(s,t)\,,\\
\tilde{F}_{QD}(s,t) &= \delta_e I^{(3)}_t F_{QD}(s,t)\,.
\end{aligned} \tag{1.11}$$

Note that *tilded* form factors absorb couplings, which leads to a compactification of formulae for the amplitude and IBA cross-section, while explicit expressions will be given for *untilded* quantities. The representation of Eq. (1.10) is very convenient for the subsequent discussion of one-loop amplitudes.

Furthermore, in Eq. (1.10) we use the Z/γ propagator ratio with an s-dependent (or constant) Z width:

$$\chi_Z(s) = \frac{1}{4s_W^2 c_W^2} \frac{s}{s - M_Z^2 + i\dfrac{\Gamma_Z}{M_Z}s}. \tag{1.12}$$

2 Building Blocks in the OMS Approach

We start our discussion by presenting various *building blocks*, used to construct the one-loop form factors of the processes $e^+e^- \to f\bar{f}$ in terms of the A_0, B_0, C_0 and D_0 functions. They are shown in order of increasing complexity: self-energies, vertices, and boxes.

2.1 Bosonic self-energies

2.1.1 Z, γ bosonic self-energies and Z–γ transition

In the R_ξ gauge there are 14 diagrams that contribute to the *total* Z and γ bosonic self-energies and to the Z–γ transition. They are shown in Fig. 2.

With S_{ZZ}, $S_{Z\gamma}$ and $S_{\gamma\gamma}$ standing for the sum of all diagrams, depicted by a grey circle in Fig. 2, we define the three corresponding self-energy functions Σ_{AB}:

$$
\begin{aligned}
S_{ZZ} &= (2\pi)^4 i \frac{g^2}{16\pi^2 c_W^2} \Sigma_{ZZ}\,, && (2.1)\\
S_{Z\gamma} &= (2\pi)^4 i \frac{g^2 s_W}{16\pi^2 c_W} \Sigma_{Z\gamma}\,, && (2.2)\\
S_{\gamma\gamma} &= (2\pi)^4 i \frac{g^2 s_W^2}{16\pi^2} \Sigma_{\gamma\gamma}\,. && (2.3)
\end{aligned}
$$

All **bosonic** self-energies and transitions may be naturally split into *bosonic* and *fermionic* components.

- Bosonic components of Z, γ self-energies and Z–γ transitions (see diagrams Fig. 2)

$$
\begin{aligned}
\Sigma^{\rm bos}_{ZZ}(s) &= M_Z^2 \Biggl\{ \frac{1}{3}\frac{1}{R_Z}\left(\frac{1}{2} - c_W^2 - 9c_W^4\right) && (2.4)\\
&\quad -\frac{3}{2}\left[\left(1+2c_W^4\right)\frac{1}{r_{HZ}} - \frac{1}{2} - c_W^2 + \frac{8}{3}c_W^4 + \frac{1}{2}r_{HZ}\right]\Biggr\}\frac{1}{\bar{\varepsilon}} + \Sigma^{{\rm bos},F}_{ZZ}(s),
\end{aligned}
$$

$$
\begin{aligned}
\Sigma^{{\rm bos},F}_{ZZ}(s) &= \frac{M_Z^2}{12}\Biggl\{\left[4c_W^2\left(5 - 8c_W^2 - 12c_W^4\right) + \left(1 - 4c_W^2 - 36c_W^4\right)\frac{1}{R_Z}\right] B_0^F(-s; M_W, M_W)\\
&\quad + \left[\frac{1}{R_Z} + 10 - 2r_{HZ} + \left(r_{HZ}-1\right)^2 R_Z\right] B_0^F(-s; M_H, M_Z)\\
&\quad + \left[\frac{18}{r_{HZ}} + 1 + \left(1 - r_{HZ}\right) R_Z\right] L_\mu(M_Z^2) + r_{HZ}\Bigl[7 - \left(1 - r_{HZ}\right) R_Z\Bigr] L_\mu(M_H^2)\\
&\quad + 2c_W^2\left(\frac{18}{r_{HW}} + 1 + 8c_W^2 - 24c_W^4\right) L_\mu(M_W^2) && (2.5)\\
&\quad + \frac{4}{3}\left(1 - 2c_W^2\right)\frac{1}{R_Z} - 6\left(1 + 2c_W^4\right)\frac{1}{r_{HZ}} - 3(1 + 2c_W^2) - 9r_{HZ} - \left(1 - r_{HZ}\right)^2 R_Z\Biggr\}.
\end{aligned}
$$

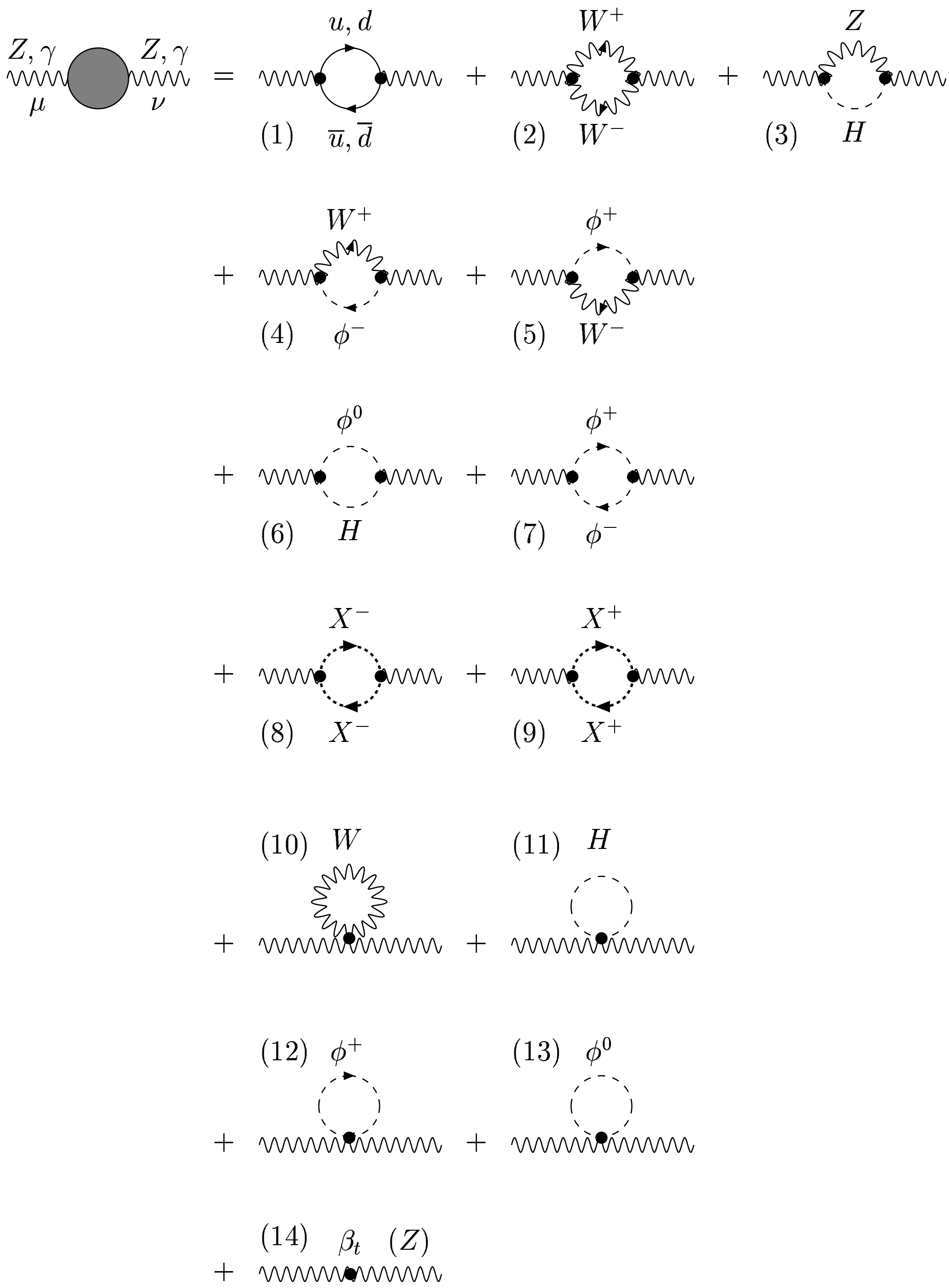

Figure 2: (Z,γ)-boson self-energy; Z–γ transition.

Here $L_\mu(M^2)$ denotes the log containing the 't Hooft scale μ:

$$L_\mu(M^2) = \ln \frac{M^2}{\mu^2} \,, \tag{2.6}$$

and it should be understood that, contrary to the one used in [7], we define here

$$B_0(-s; M_1, M_2) = \frac{1}{\bar{\varepsilon}} + B_0^F(-s; M_1, M_2), \tag{2.7}$$

meaning that B_0^F also depends on the scale μ. We will not explicitly maintain μ in the arguments list of L_μ and B_0^F. Leaving μ unfixed, we retain an opportunity to control μ independence (and therefore UV finiteness) in numerical realization of one-loop form factors, providing thereby an additional cross-check.

Next, it is convenient to introduce the dimensionless quantities $\Pi^{\text{bos}}_{Z\gamma}(s)$ and $\Pi^{\text{bos}}_{\gamma\gamma}(s)$ (vacuum polarizations):

$$\Sigma^{\text{bos}}_{Z\gamma}(s) = -s\Pi^{\text{bos}}_{Z\gamma}(s), \tag{2.8}$$

$$\Sigma^{\text{bos}}_{\gamma\gamma}(s) = -s\Pi^{\text{bos}}_{\gamma\gamma}(s). \tag{2.9}$$

In Eqs. (2.5) and (2.7) and below, the following abbreviations are used:

$$c^2_W = \frac{M^2_W}{M^2_Z} \,, \qquad r_{ij} = \frac{m^2_i}{m^2_j} \,, \qquad R_W = \frac{M^2_W}{s} \,, \qquad R_Z = \frac{M^2_Z}{s} \,. \tag{2.10}$$

Since only finite parts will contribute to resulting expressions for physical amplitudes, which should be free from ultraviolet poles, it is convenient to split every divergent function into singular and finite parts:

$$\Pi^{\text{bos}}_{\gamma\gamma}(s) = 3\frac{1}{\bar{\varepsilon}} + \Pi^{\text{bos},F}_{\gamma\gamma}(s), \tag{2.11}$$

$$\Pi^{\text{bos},F}_{\gamma\gamma}(s) = (3 + 4R_W)\, B_0^F(-s; M_W, M_W) + 4R_W L_\mu(M^2_W), \tag{2.12}$$

and

$$\Pi^{\text{bos}}_{Z\gamma}(s) = \left(\frac{1}{6} + 3c^2_W + 2R_W\right) \frac{1}{\bar{\varepsilon}} + \Pi^{\text{bos},F}_{Z\gamma}(s), \tag{2.13}$$

$$\begin{aligned}\Pi^{\text{bos},F}_{Z\gamma}(s) &= \left[\frac{1}{6} + 3c^2_W + 4\left(\frac{1}{3} + c^2_W\right) R_W\right] B_0^F(-s; M_W, M_W) \\ &\quad + \frac{1}{9} - \left(\frac{2}{3} - 4c^2_W\right) R_W L_\mu(M^2_W).\end{aligned} \tag{2.14}$$

With the Z boson self-energy, Σ_{ZZ}, we construct a useful ratio:

$$\mathcal{D}_Z(s) = \frac{1}{c^2_W} \frac{\Sigma_{ZZ}(s) - \Sigma_{ZZ}(M^2_Z)}{M^2_Z - s} \,, \tag{2.15}$$

which also has bosonic and fermionic parts. The bosonic component is:

$$\mathcal{D}_Z^{\rm bos}(s) = \frac{1}{c_W^2}\left(-\frac{1}{6}+\frac{1}{3}c_W^2+3c_W^4\right)\frac{1}{\bar{\varepsilon}}+\mathcal{D}_Z^{{\rm bos},F}(s)\,, \tag{2.16}$$

$$\begin{aligned}\mathcal{D}_Z^{{\rm bos},F}(s) = \frac{1}{c_W^2}\Biggl\{&\left(\frac{1}{12}+\frac{4}{3}c_W^2-\frac{17}{3}c_W^4-4c_W^6\right)\\ &\times\frac{M_Z^2}{M_Z^2-s}\left[B_0^F(-s;M_W,M_W)-B_0^F(-M_Z^2;M_W,M_W)\right]\\ &-\left(\frac{1}{12}-\frac{1}{3}c_W^2-3c_W^4\right)B_0^F(-s;M_W,M_W)\\ &+\left(1-\frac{1}{3}r_{HZ}+\frac{1}{12}r_{HZ}^2\right)\frac{M_Z^2}{M_Z^2-s}\left[B_0^F(-s;M_H,M_Z)-B_0^F(-M_Z^2;M_H,M_Z)\right]\\ &-\frac{1}{12}\left[1-(1-r_{HZ})^2R_Z\right]B_0^F(-s;M_H,M_Z)\\ &-\frac{1}{12}R_Z(1-r_{HZ})\left[r_{HZ}\left(L_\mu(M_H^2)-1\right)-L_\mu(M_Z^2)+1\right]-\frac{1}{9}\left(1-2c_W^2\right)\Biggr\}.\end{aligned} \tag{2.17}$$

- Fermionic components of the Z and γ bosonic self-energies and of the Z–γ transition

These are represented as sums over all fermions of the theory, $\sum_f$. They, of course, depend on vector and axial couplings of fermions to the Z boson, v_f and a_f, and to the photon, electric charge eQ_f, as well as on the colour factor c_f and fermion mass m_f. The couplings are defined as usual:

$$v_f = I_f^{(3)} - 2Q_f s_W^2\,, \qquad a_f = I_f^{(3)}, \tag{2.18}$$

with weak isospin $I_f^{(3)}$, and

$$Q_f = -1 \quad \text{for leptons,} \quad +\frac{2}{3} \quad \text{for up quarks,} \quad -\frac{1}{3} \quad \text{for down quarks,} \tag{2.19}$$

$$c_f = 1 \quad \text{for leptons,} \quad 3 \quad \text{for quarks.} \tag{2.20}$$

The three main self-energy functions are:

$$\Sigma_{ZZ}^{\rm fer}(s) = \sum_f c_f\left[-\left(v_f^2+a_f^2\right)sB_f(-s;m_f,m_f)-2a_f^2m_f^2B_0(-s;m_f,m_f)\right], \tag{2.21}$$

$$\Sigma_{\gamma\gamma}^{\rm fer}(s) = -s\Pi_{\gamma\gamma}^{\rm fer}(s), \tag{2.22}$$

$$\Sigma_{Z\gamma}^{\rm fer}(s) = -s\Pi_{Z\gamma}^{\rm fer}(s)\,. \tag{2.23}$$

The quantities $\Pi_{\gamma\gamma}^{\rm fer}$ and $\Pi_{Z\gamma}^{\rm fer}$ are different according to different couplings, but proportional to one function B_f (see Eq. (5.252) of [7] for its definition):

$$\Pi_{\gamma\gamma}^{\rm fer}(s) = 4\sum_f c_f\,Q_f^2\,B_f(-s;m_f,m_f)\,, \tag{2.24}$$

$$\Pi_{Z\gamma}^{\rm fer}(s) = 2\sum_f c_f\,Q_f\,v_f\,B_f(-s;m_f,m_f)\,. \tag{2.25}$$

As usual, we subdivided them into singular and finite parts:

$$\Pi^{\rm fer}_{Z\gamma}(s) = -\frac{1}{3}\left(\frac{1}{2}N_f - 4s^2_{W}\sum_f c_f Q^2_f\right)\frac{1}{\bar{\varepsilon}} + \Pi^{{\rm fer},F}_{Z\gamma}(s), \tag{2.26}$$

$$\Sigma^{\rm fer}_{ZZ}(s) = \left\{-\frac{1}{2}\sum_f c_f m^2_f + \frac{s}{3}\left[\left(\frac{1}{2} - s^2_{W}\right)N_f + 4s^4_{W}\sum_f c_f Q^2_f\right]\right\}\frac{1}{\bar{\varepsilon}} + \Sigma^{{\rm fer},F}_{ZZ}(s).$$

In Eq. (2.26), $N_f = 24$ is the total number of fermions in the SM. We do not show explicit expressions for finite parts, marked with superscript F, because these might be trivially derived from Eq. (2.21) and Eqs. (2.24), (2.25) by replacing complete expressions for B_f and B_0 with their finite parts B^F_f and B^F_0, correspondingly.

2.1.2 W boson self-energy

Next we consider the W boson self-energy, which is described, in the R_ξ gauge, by 16 diagrams, shown in Fig. 3.

First, we present an explicit expression for its bosonic component:

$$\Sigma^{\rm bos}_{WW}(s) = M^2_{W}\left\{-\frac{19}{6}\frac{1}{R_W} - \frac{1}{4}\left[\frac{6}{r_{HW}}\left(\frac{1}{c^4_{W}}+2\right) - \frac{3}{c^2_{W}} + 10 + 3r_{HW}\right]\right\}\frac{1}{\bar{\varepsilon}} + \Sigma^{{\rm bos},F}_{WW}(s), \tag{2.27}$$

where

$$\begin{aligned}
\Sigma^{{\rm bos},F}_{WW}(s) = \frac{M^2_{W}}{12}\Biggl\{ & \left[\left(1-40c^2_{W}\right)\frac{1}{R_W} + 2\left(\frac{5}{c^2_{W}} - 27 - 8c^2_{W}\right)\right. \\
& \left. +\frac{s^4_{W}}{c^2_{W}}\left(\frac{1}{c^2_{W}}+8\right)R_W\right]B_0(-s;M_W,M_Z) \\
& +\left[\frac{1}{R_W} + 2\left(5-r_{HW}\right) + \left(1-r_{HW}\right)^2 R_W\right]B_0(-s;M_W,M_H) \\
& -8s^2_{W}\left(\frac{5}{R_W} + 2 - R_W\right)B_0(-s;M_W,0) \\
& +r_{HW}\left[7-\left(1-r_{HW}\right)R_W\right]L_\mu(M^2_H) \\
& +\frac{1}{c^2_{W}}\left[\frac{18}{r_{HW}}\frac{1}{c^2_{W}} + 1 - 16c^2_{W} + s^2_{W}\left(\frac{1}{c^2_{W}}+8\right)R_W\right]L_\mu(M^2_Z) \\
& +\left[2\left(\frac{18}{r_{HW}} - 7\right) - \left(\frac{1}{c^2_{W}} - 2 + r_{HW}\right)R_W\right]L_\mu(M^2_W) \\
& -\frac{4}{3}\frac{1}{R_W} - 12\left(\frac{1}{2}\frac{1}{c^4_{W}}+1\right)\frac{1}{r_{HW}} - 3\left(\frac{1}{c^2_{W}}+2\right) - 9r_{HW} \\
& -\left[\left(\frac{1}{c^2_{W}} + 6s^2_{W}\right)\frac{1}{c^2_{W}} - r_{HW}\left(2-r_{HW}\right)\right]R_W\Biggr\}.
\end{aligned} \tag{2.28}$$

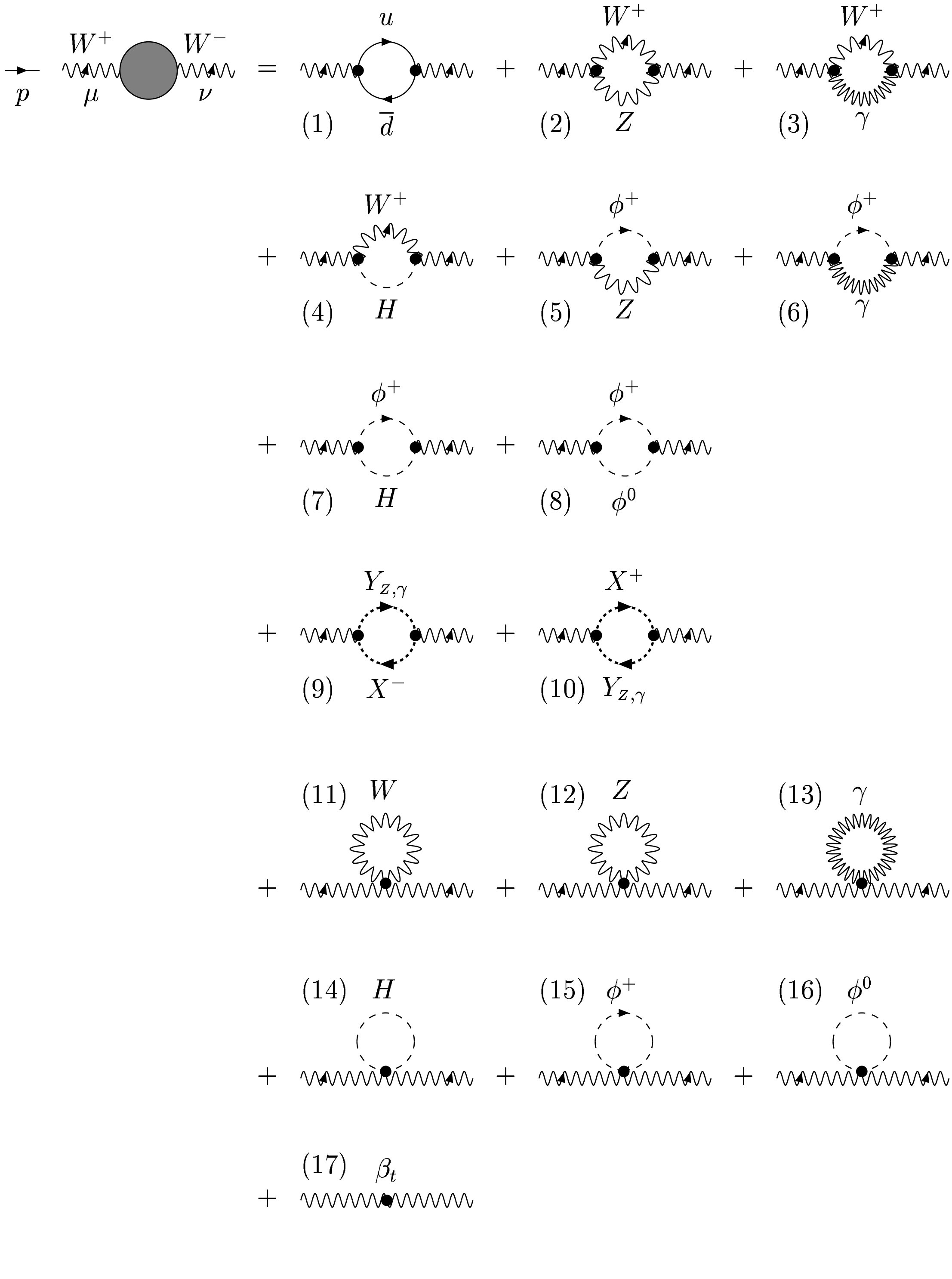

Figure 3: W boson self-energy.

Secondly, we give its fermionic component:

$$\Sigma^{\rm fer}_{WW}(s) \;=\; -s\sum_{f=d} c_f B_f(-s;m_{f'},m_f) + \sum_f c_f m_f^2 B_1(-s;m_{f'},m_f), \tag{2.29}$$

where summation in the first term extends to all *doublets* of the SM.

2.1.3 Bosonic self-energies and counterterms

Bosonic self-energies and transitions enter one-loop amplitudes either directly through the functions $\mathcal{D}_Z(s)$, $\Pi_{\gamma\gamma}(s)$ and $\Pi_{Z\gamma}(s)$, or by means of bosonic counterterms, which are made of self-energy functions at zero argument, owing to *electric charge renormalization*, or at $p^2=-M^2$, that is on a mass shell, owing to *on-mass-shell renormalization* (OMS scheme).

- Electric charge renormalization

The electric charge renormalization introduces the quantity $z_\gamma - 1$:

$$(z_\gamma - 1) = s^2_W\left[\Pi_{\gamma\gamma}(0) - \frac{2}{M^2_W}\overline{\Sigma}_{3Q}(0)\right], \tag{2.30}$$

with bosonic (see Eq. (6.161) of [7]):

$$(z_\gamma - 1)^{\rm bos} = s^2_W\left[3\Big(\frac{1}{\bar\varepsilon} - L_\mu(M^2_W)\Big) + \frac{2}{3}\right], \tag{2.31}$$

and fermionic

$$(z_\gamma - 1)^{\rm fer} \;=\; s^2_W\left[\Big(-\frac{4}{3}\sum_f c_f Q^2_f\Big)\frac{1}{\bar\varepsilon} + \Pi^{{\rm fer},F}_{\gamma\gamma}(0)\right] \tag{2.32}$$

components.

- ρ-parameter

Finally, two self-energy functions enter Veltman's parameter $\Delta\rho$, a gauge-invariant combination of self-energies, which naturally appears in the one-loop calculations:

$$\Delta\rho \;=\; \frac{1}{M^2_W}\left[\Sigma_{WW}(M^2_W) - \Sigma_{ZZ}(M^2_Z)\right], \tag{2.33}$$

with individual components where we explicitly show the pole parts:

$$\Delta\rho^{\rm bos} \;=\; \left(-\frac{1}{6c^2_W} - \frac{41}{6} + 7c^2_W\right)\frac{1}{\bar\varepsilon} + \Delta\rho^{{\rm bos},F}, \tag{2.34}$$

$$\Delta\rho^{\rm fer} \;=\; \frac{1}{3}\frac{s^2_W}{c^2_W}\left(\frac{1}{2}N_f - 4s^2_W\sum_f c_f Q^2_f\right)\frac{1}{\bar\varepsilon} + \Delta\rho^{{\rm fer},F}. \tag{2.35}$$

The finite part of $\Delta\rho^{\rm bos}$ is given explicitly by

$$
\begin{aligned}
\Delta\rho^{{\rm bos},F} \; = \; & \left(\frac{1}{12c_W^4}+\frac{4}{3c_W^2}-\frac{17}{3}-4c_W^2\right)\left[B_0^F(-M_W^2;M_W,M_Z)-c_W^2 B_0^F(-M_Z^2;M_W,M_W)\right] \\
& +\left(1-\frac{1}{3}r_{HW}+\frac{1}{12}r_{HW}^2\right)B_0^F(-M_W^2;M_W,M_H) \\
& -\left(1-\frac{1}{3}r_{HZ}+\frac{1}{12}r_{HZ}^2\right)\frac{1}{c_W^2}B_0^F(-M_Z^2;M_Z,M_H)-4s_W^2 B_0^F(-M_W^2;M_W,0) \\
& +\frac{1}{12}\Biggl[\left(\frac{1}{c_W^4}+\frac{6}{c_W^2}-24+r_{HW}\right)L_\mu(M_Z^2)+s_W^2 r_{HW}^2\left[L_\mu(M_H^2)-1\right] \\
& -\left(\frac{1}{c_W^2}+14+16c_W^2-48c_W^4+r_{HW}\right)L_\mu(M_W^2)-\frac{1}{c_W^4}-\frac{19}{3c_W^2}+\frac{22}{3}\Biggr], \qquad (2.36)
\end{aligned}
$$

while the finite part of $\Delta\rho^{\rm fer}$ is not shown, since it is trivially derived from the defining equation (2.33) by replacing the total self-energies with their finite parts.

2.2 Fermionic self-energies

2.2.1 Fermionic self-energy diagrams

The total self-energy function of a fermion in the R_ξ gauge is described by the six diagrams of Fig. 4.

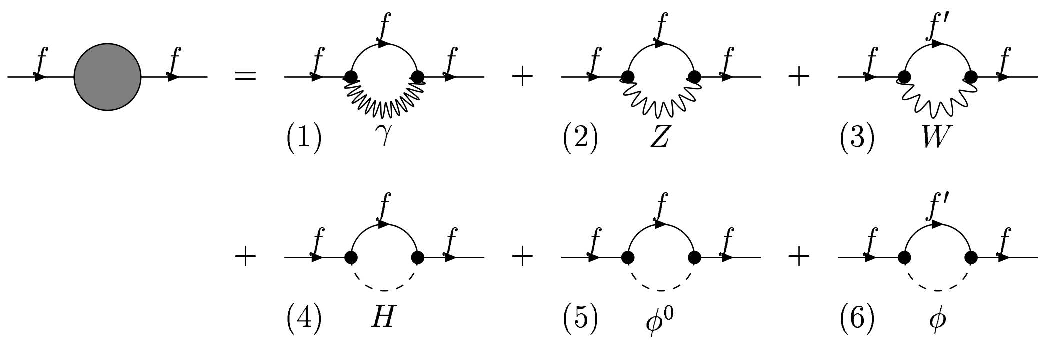

Figure 4: Fermionic self-energy diagrams.

Calculating derivatives straightforwardly and substituting the a_i's, we obtain (see [6]) explicit expressions for the wave-function renormalization factor $\sqrt{z_{L,R}}$.

It is convenient to distinguish the electromagnetic components

$$
\left(\sqrt{z_L}-I\right)_f^{em} \; = \; \left(\sqrt{z_R}-I\right)_f^{em}=s_W^2 Q_f^2\left(-\frac{1}{2\bar{\varepsilon}}+\frac{1}{\hat{\varepsilon}}+\frac{3}{2}\ln\frac{m_f^2}{\mu^2}-2\right) \qquad (2.37)
$$

and the weak components

$$
\left|\sqrt{z_{L,R}}\right|-I=\left(w_v\pm w_a\right), \qquad (2.38)
$$

where

$$
\begin{aligned}
w_v^Z &= -\frac{1}{8}\frac{1}{c_W^2}\Bigg\{\left(v_t^2+a_t^2+2a_t^2 r_{tz}\right)\frac{1}{\bar{\varepsilon}}+\left(v_t^2+a_t^2\right)\left[\frac{1}{r_{tz}}\left(B_0^F(-m_t^2;M_Z,m_t)+L_\mu(M_Z^2)-1\right)\right.\\
&\left. +2\left(1+2r_{tz}\right)M_Z^2 B_{0p}(-m_t^2;m_t,M_Z)-L_\mu(m_t^2)\right]+2a_t^2 r_{tz}\left[\frac{1}{r_{tz}}\Big(B_0^F(-m_t^2;M_Z,m_t)\right.\\
&\left. +L_\mu(M_Z^2)-1\Big)-6M_Z^2 B_{0p}(-m_t^2;m_t,M_Z)-L_\mu(m_t^2)+1\right]\Bigg\}, \qquad (2.39)\\
w_v^W &= -\frac{1}{16}\left(2+r_{tw}\right)\Bigg\{\frac{1}{\bar{\varepsilon}}+\frac{1+r_{tw}}{r_{tw}}\left[B_0^F(-m_t^2;M_W,0)-1\right]\\
&+2\left(1-r_{tw}\right)M_W^2 B_{0p}(-m_t^2;0,M_W)+\frac{1}{4r_{tw}}L_\mu(M_W^2)\Bigg\}+r_{tw}\,, \qquad (2.40)\\
w_v^H &= -\frac{1}{16}r_{tw}\Bigg\{\frac{1}{\bar{\varepsilon}}+r_{Ht}\left[B_0^F(-m_t^2;M_H,m_t)+L_\mu(M_H^2)-1\right]\\
&-2\left(4r_{tH}-1\right)M_H^2 B_{0p}(-m_t^2;m_t,M_H)-L_\mu(m_t^2)+1\Bigg\}, \qquad (2.41)\\
w_a^Z &= -\frac{1}{4c_W^2}v_t a_t\Bigg\{\frac{1}{\bar{\varepsilon}}-\frac{1}{r_{tz}}\left[B_0^F(-m_t^2;M_Z,m_t)+L_\mu(M_Z^2)-1\right]\\
&+2B_0^F(-m_t^2;M_Z,m_t)+L_\mu(m_t^2)-2\Bigg\}, \qquad (2.42)\\
w_a^W &= -\frac{1}{16}\Bigg\{\left(2-r_{tw}\right)\frac{1}{\bar{\varepsilon}}-\left(\frac{2}{r_{tw}}-3\right)\left[B_0^F(-m_t^2;M_W,0)-1\right]\\
&-r_{tw}B_0^F(-m_t^2;M_W,0)-\left(\frac{2}{r_{tw}}-1\right)L_\mu(M_W^2)\Bigg\}. \qquad (2.43)
\end{aligned}
$$

2.3 The $Zf\bar{f}$ and $\gamma f\bar{f}$ vertices

Consider now the sum of all vertices and corresponding counterterms whose contribution originates from the fermionic self-energy diagrams of Fig. 4. This sum is shown in Fig. 5.

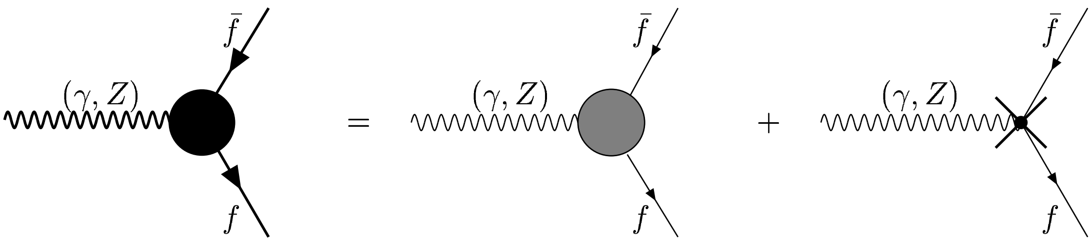

Figure 5: *$Zf\bar{f}$ and $\gamma f\bar{f}$ vertices with fermionic counterterms.*

The formulae which determine the counterterms are:

$$
F_Q^{\gamma,ct} = 2\left(\sqrt{z_R}-I\right), \qquad (2.44)
$$

$$F_L^{\gamma,ct} = (\sqrt{z_L} - I) - (\sqrt{z_R} - I)\,, \tag{2.45}$$
$$F_Q^{z,ct} = \delta_f^2\,(\sqrt{z_R} - I)\,, \tag{2.46}$$
$$F_L^{z,ct} = \sigma_f^2\,(\sqrt{z_R} - I) - \delta_f^2\,(\sqrt{z_R} - I)\,, \tag{2.47}$$

where

$$\delta_f = v_f - a_f, \qquad \sigma_f = v_f + a_f. \tag{2.48}$$

For the sum of all $\gamma \to f\bar{f}$ and $Z \to f\bar{f}$ vertices (the *total* $\gamma(Z)f\bar{f}$ vertex depicted by a grey circle in Fig. 5) we use the standard normalization

$$i\pi^2 = (2\pi)^4\, i\frac{1}{16\pi^2}\,, \tag{2.49}$$

and define

$$V_\mu^\gamma(s) = (2\pi)^4\, i\frac{1}{16\pi^2} G_\mu(s)\,, \tag{2.50}$$
$$V_\mu^Z(s) = (2\pi)^4\, i\frac{1}{16\pi^2} Z_\mu(s)\,, \tag{2.51}$$

while we denote the individual vertices as follows:

$$G_\mu(s) = G_\mu^\gamma(s) + G_\mu^Z(s) + G_\mu^W(s) + G_\mu^H(s)\,, \tag{2.52}$$
$$Z_\mu(s) = Z_\mu^\gamma(s) + Z_\mu^Z(s) + Z_\mu^W(s) + Z_\mu^H(s)\,. \tag{2.53}$$

All vertices have three components in our LQD basis.

2.3.1 Scalar form factors

Now we construct the $24 = (4 : A, Z, H, W\text{-virtual}) \otimes (3 : L, Q, D) \otimes (2 : \gamma, Z\text{-incoming})$ scalar form factors, originating from the diagrams of Fig. 5. They are derived from the following six equations — three projections for $\gamma f\bar{f}$ vertices:

$$F_L^{\gamma B}(s) = \frac{2}{s_W I_f^{(3)}}\Big\{G_\mu^B(s)\,[ig^3\gamma_\mu\gamma_+] + s_W Q_f F_L^{\gamma,ct}\Big\}, \tag{2.54}$$
$$F_Q^{\gamma B}(s) = \frac{1}{s_W Q_f}\Big\{G_\mu^B(s)\,[ig^3\gamma_\mu] + s_W Q_f F_Q^{\gamma,ct}\Big\}, \tag{2.55}$$
$$F_D^{\gamma B}(s) = \frac{2}{s_W I_t^{(3)}} G_\mu^B(s)\,[g^3 m_t I D_\mu]\,, \tag{2.56}$$

and three projections for $Zf\bar{f}$ vertices:

$$F_L^{zB}(s) = \frac{2c_W}{I_f^{(3)}}\left\{Z_\mu^B(s)\,[ig^3\gamma_\mu\gamma_+] + \frac{1}{c_W}F_L^{z,ct}\right\}, \tag{2.57}$$
$$F_Q^{zB}(s) = \frac{2c_W}{\delta_f}\left\{Z_\mu^B(s)\,[ig^3\gamma_\mu] + \frac{1}{c_W}F_Q^{z,ct}\right\}, \tag{2.58}$$
$$F_D^{zB}(s) = \frac{2c_W}{I_t^{(3)}} Z_\mu^B(s)\,[g^3 m_t I D_\mu]\,. \tag{2.59}$$

Here we have $f = t, e$, and $B = A, Z, W, H$, and we introduce the symbol $[\ldots]$ for the definition of the procedure of the projection of $G_\mu(s)$ and $Z_\mu(s)$ to our basis. It has the same meaning as in `form` language [20], namely, e.g. $G^B_\mu(s)\,[ig^3\gamma_\mu\gamma_+]$ means that only the coefficient of $[ig^3\gamma_\mu\gamma_+]$ of the whole expression $G^B_\mu(s)$ is taken (*projected*).

The factors $1/(Q_f s_W)$, $2/(s_W I^{(3)}_t)$ and $2c^2_W/(s_W I^{(3)}_t)$ for $\gamma f\bar{f}$ vertices, and the factors $2c_W/I^{(3)}_t$, $2c_W/\delta_f$ and $2c_W/I^{(3)}_t$ for $Zf\bar{f}$ are due to the form factor definitions of Eq. (1.10).

The total $\gamma t\bar{t}$ and $Zt\bar{t}$ form factors are sums over three bosonic contributions $B = Z, W, H$ since we separated out the contribution of the diagram with virtual $\gamma \equiv A$:

$$\begin{aligned}
F^{\gamma tt}_{L}(s) &= F^{\gamma Z}_{L}(s) + F^{\gamma W}_{L}(s)\,,\\
F^{\gamma tt}_{Q}(s) &= F^{\gamma Z}_{Q}(s) + F^{\gamma W}_{Q}(s) + F^{\gamma H}_{Q}(s)\,,\\
F^{\gamma tt}_{D}(s) &= F^{\gamma Z}_{D}(s) + F^{\gamma W}_{D}(s) + F^{\gamma H}_{D}(s)\,,\\
F^{Ztt}_{L}(s) &= F^{ZZ}_{L}(s) + F^{ZW}_{L}(s) + F^{ZH}_{L}(s)\,,\\
F^{Ztt}_{Q}(s) &= F^{ZZ}_{Q}(s) + F^{ZW}_{Q}(s) + F^{ZH}_{Q}(s)\,,\\
F^{Ztt}_{D}(s) &= F^{ZZ}_{D}(s) + F^{ZW}_{D}(s) + F^{ZH}_{D}(s)\,.
\end{aligned} \tag{2.60}$$

The quantities $F^{\gamma(Z)B}_{L,Q,D}(s)$ originate from groups of diagrams, which we will call *clusters*.

2.4 Library of form factors for Btt clusters

Here we present a complete collection of scalar form factors $F^{\gamma(Z)B}_{L,Q,D}(s)$ originating from a vertex diagram with a virtual vector boson, contribution of a scalar partner of this vector boson, and relevant counterterms.

Actually three gauge-invariant subsets of diagrams of this kind, A, Z and H, appear in our calculation. They may be termed *clusters*, since they are natural building blocks of the complete scalar form factors, which are the aim of our calculation. Again, in the spirit of our presentation, we write down their pole and finite parts. The remaining vertices with virtual W and ϕ^+, ϕ^- with relevant counterterms we also define as the W cluster. However, the latter diagrams do not form a gauge-invariant subset.

2.4.1 Form factors of the Z cluster

The diagrams shown in Fig. 6 contribute to the Z cluster.

Separating out pole contributions $1/\bar{\varepsilon}$, we define finite (calligraphic) quantities. We note that, if a form factor $F^{ij}_A(s)$ has a pole, then the corresponding finite part $\mathcal{F}^{ij}_A(s)$ is μ-dependent:

$$\begin{aligned}
F^{\gamma Z}_{L}(s) &= \mathcal{F}^{\gamma Z}_{L}(s)\,,\\
F^{\gamma Z}_{Q}(s) &= \mathcal{F}^{\gamma Z}_{Q}(s)\,,\\
F^{\gamma Z}_{D}(s) &= \mathcal{F}^{\gamma Z}_{D}(s)\,,\\
F^{ZZ}_{L}(s) &= -\frac{1}{4} r_{tw} \frac{1}{\bar{\varepsilon}} + \mathcal{F}^{ZZ}_{L}(s)\,,\\
F^{ZZ}_{Q}(s) &= -\frac{1}{16} \frac{1}{|Q_t|\, s^2_W} r_{tw} \frac{1}{\bar{\varepsilon}} + \mathcal{F}^{ZZ}_{Q}(s)\,,
\end{aligned}$$

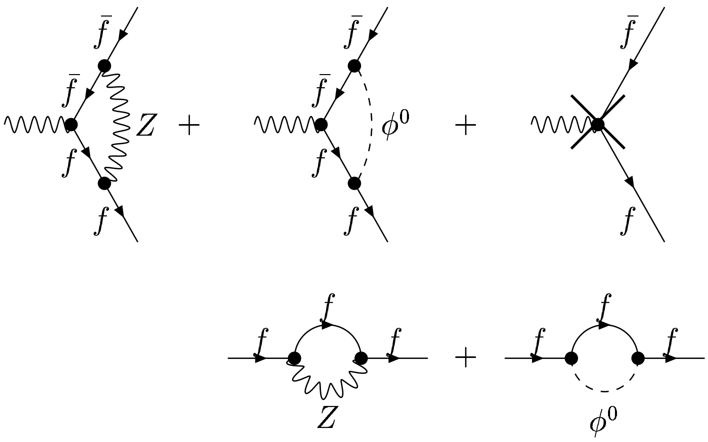

Figure 6: Z cluster. The two fermionic self-energy diagrams in the second row give rise to the counterterm contribution depicted by the solid cross in the last diagram of the first row.

$$F_{D}^{zZ}(s) = \mathcal{F}_{D}^{zZ}(s)\,. \tag{2.61}$$

Here the finite parts are:

$$\begin{aligned}\mathcal{F}_{L}^{\gamma Z}(s) = {} & \frac{1}{c_W^2} Q_t v_t \Bigg\{ 2\left(2+\frac{1}{R_Z}\right) M_Z^2 C_0(-m_t^2, -m_t^2, -s; m_t, M_Z, m_t) \\ & -3B_0^F(-s; m_t, m_t) + 2B_0^F(-m_t^2; m_t, M_Z) - L_\mu(m_t^2) \\ & + B_{d1}^F(-m_t^2; m_t, M_Z) - 2(1+4r_{tZ}) \frac{M_Z^2}{\Delta_{3r}} L_{ab}(m_t, m_t, M_Z) \Bigg\},\end{aligned} \tag{2.62}$$

$$\begin{aligned}\mathcal{F}_{Q}^{\gamma Z}(s) = {} & \frac{1}{4c_W^2} \Bigg\{ \delta_t^2 \Bigg[2\left(2(1-r_{tZ})+\frac{1}{R_Z}\right) M_Z^2 C_0(-m_t^2, -m_t^2, -s; m_t, M_Z, m_t) \\ & -3B_0^F(-s; m_t, m_t) + 4B_0^F(-m_t^2; m_t, M_Z) + L_\mu(M_Z^2) - r_{tZ} B_{d2}^F(-m_t^2; m_t, M_Z) \\ & -2(1+2r_{tZ}) M_Z^2 B_{0p}(-m_t^2; m_t, M_Z) - \frac{5}{2} \Bigg] \\ & +2v_t a_t r_{tZ} \Bigg[-4M_Z^2 C_0(-m_t^2, -m_t^2, -s; m_t, M_Z, m_t) + 2\left(L_\mu(m_t^2) - L_\mu(M_Z^2)\right) \\ & -2(1-r_{tZ}) B_{d2}^F(-m_t^2; m_t, M_Z) + 1 \\ & -\frac{2}{r_{tZ}} \left((1+2r_{tZ}) M_Z^2 B_{0p}(-m_t^2; m_t, M_Z) + \frac{1}{2} \right) \Bigg] \\ & +2a_t^2 r_{tZ} \Bigg[B_0^F(-s; m_t, m_t) + L_\mu(M_Z^2) - r_{tZ} B_{d2}^F(-m_t^2; m_t, M_Z) \\ & +6M_Z^2 B_{0p}(-m_t^2; m_t, M_Z) - \frac{5}{2} \Bigg] \\ & -4\left[\frac{\delta_t^2}{2} - \left(4v_t a_t - a_t^2\right) r_{tZ} \right] \frac{M_Z^2}{\Delta_{3r}} L_{ab}(m_t, m_t, M_Z) \Bigg\},\end{aligned} \tag{2.63}$$

$$
\begin{aligned}
\mathcal{F}^{\gamma Z}_{D}(s) &= -\frac{2Q_t}{I^{(3)}_t c^2_W}\frac{1}{\Delta_{3r}}\Biggl\{\frac{v^2_t+a^2_t}{2}\Biggl[-4M^2_Z C_0(-m^2_t,-m^2_t,-s;m_t,M_Z,m_t)\\
&+B^F_0(-s;m_t,m_t)-2B^F_0(-m^2_t;m_t,M_Z)-L_\mu(m^2_t)+B^F_{d1}(-m^2_t;m_t,M_Z)\\
&+2+6\frac{M^2_Z}{\Delta_{3r}}L_{ab}(m_t,m_t,M_Z)\Biggr]\\
&+a^2_t\Biggl[2\left(3r_{tZ}-\frac{1}{R_Z}\right)M^2_Z C_0(-m^2_t,-m^2_t,-s;m_t,M_Z,m_t)\\
&+B^F_0(-m^2_t;m_t,M_Z)+L_\mu(M^2_Z)-1-r_{tZ}\Bigl[B^F_0(-s;m_t,m_t)+L_\mu(m^2_t)-2\Bigr]\\
&-2\left(2-3\frac{m^2_t}{\Delta_{3r}}\right)L_{ab}(m_t,m_t,M_Z)\Biggr]\Biggr\},
\end{aligned}
\tag{2.64}
$$

$$
\begin{aligned}
\mathcal{F}^{ZZ}_{L}(s) &= \frac{1}{4c^2_W}\Biggl\{\frac{3v^2_t+a^2_t}{3}\Biggl[2\left(3\left(2+\frac{1}{R_Z}\right)-2r_{tZ}\right)M^2_Z C_0(-m^2_t,-m^2_t,-s;m_t,M_Z,m_t)\\
&-9B^F_0(-s;m_t,m_t)+8B^F_0(-m^2_t;m_t,M_Z)-L_\mu(m^2_t)\\
&+B^F_{d1}(-m^2_t;m_t,M_Z)-2\left(1+2r_{tZ}\right)M^2_Z B_{0p}(-m^2_t;m_t,M_Z)-2\Biggr]\\
&-\frac{2}{3}a^2_t\Biggl[4m^2_t C_0(-m^2_t,-m^2_t,-s;m_t,M_Z,m_t)+3r_{tZ}\Bigl[B^F_0(-s;m_t,m_t)+L_\mu(m^2_t)\Bigr]\\
&+B^F_0(-m^2_t;m_t,M_Z)+3L_\mu(M^2_Z)+2L_\mu(m^2_t)\\
&+2B^F_{d1}(-m^2_t;m_t,M_Z)+2\left(1-7r_{tZ}\right)M^2_Z B_{0p}(-m^2_t;m_t,M_Z)-1\Biggr]\\
&-2\left[\left(3v^2_t+a^2_t\right)\left(1+4r_{tZ}\right)-2a^2_t r_{tZ}\right]\frac{M^2_Z}{\Delta_{3r}}L_{ab}(m_t,m_t,M_Z)\Biggr\},
\end{aligned}
\tag{2.65}
$$

$$
\begin{aligned}
\mathcal{F}^{ZZ}_{Q}(s) &= \frac{1}{c^2_W}\Biggl\{\frac{1}{4}\delta^2_t\Biggl[2\left(2-2r_{tZ}+\frac{1}{R_Z}\right)M^2_Z C_0(-m^2_t,-m^2_t,-s;m_t,M_Z,m_t)\\
&-3B^F_0(-s;m_t,m_t)+4B^F_0(-m^2_t;m_t,M_Z)+L_\mu(m^2_t)-B^F_{d1}(-m^2_t;m_t,M_Z)\\
&-2\left(1+2r_{tZ}\right)M^2_Z B_{0p}(-m^2_t;m_t,M_Z)-2-2\frac{M^2_Z}{\Delta_{3r}}L_{ab}(m_t,m_t,M_Z)\Biggr]\\
&+a_t r_{tZ}\Biggl(v_t\Biggl[-2M^2_Z C_0(-m^2_t,-m^2_t,-s;m_t,M_Z,m_t)\\
&+\frac{1}{r_{tZ}}\Bigl[B^F_0(-m^2_t;m_t,M_Z)+L_\mu(m^2_t)-1-B^F_{d1}(-m^2_t;m_t,M_Z)\\
&-\left(1+2r_{tZ}\right)M^2_Z B_{0p}(-m^2_t;m_t,M_Z)\Bigr]+6\frac{M^2_Z}{\Delta_{3r}}L_{ab}(m_t,m_t,M_Z)\Biggr]
\end{aligned}
$$

$$
\begin{aligned}
&-\frac{1}{2}a_t\Big[8M_Z^2C_0(\,-m_t^2,-m_t^2,-s;m_t,M_Z,m_t)\\
&-B_0^F(\,-s;m_t,m_t)-L_\mu(m_t^2)+2+B_{d1}^F(\,-m_t^2;m_t,M_Z)\\
&-6M_Z^2B_{0p}(\,-m_t^2;m_t,M_Z)-10\frac{M_Z^2}{\Delta_{3r}}L_{ab}\left(m_t,m_t,M_Z\right)\Big]\\
&-\frac{a_t^2}{\delta_t}\Big[4M_Z^2C_0(\,-m_t^2,-m_t^2,-s;m_t,M_Z,m_t)\\
&-B_0^F(\,-s;m_t,m_t)+1-6\frac{M_Z^2}{\Delta_{3r}}L_{ab}\left(m_t,m_t,M_Z\right)\Big]\Big)\Big\},
\end{aligned}
\tag{2.66}
$$

$$
\begin{aligned}
\mathcal{F}_D^{zZ}\left(s\right) \;=\;& -\frac{1}{2I_t^{(3)}c_W^2}\frac{1}{\Delta_{3r}}\Big\{\left(3a_t^2+v_t^2\right)v_t\Big[-4M_Z^2C_0(\,-m_t^2,-m_t^2,-s;m_t,M_Z,m_t)\\
&+B_0^F(\,-s;m_t,m_t)-2B_0^F(\,-m_t^2;m_t,M_Z)-L_\mu(m_t^2)+B_{d1}^F(\,-m_t^2;m_t,M_Z)\\
&+2+6\frac{M_Z^2}{\Delta_{3r}}L_{ab}\left(m_t,m_t,M_Z\right)\Big]\\
&+2v_ta_t^2\Big[2\left(7r_{tZ}-2\frac{1}{R_Z}\right)M_Z^2C_0(\,-m_t^2,-m_t^2,-s;m_t,M_Z,m_t)\\
&+B_0^F(\,-m_t^2;m_t,M_Z)+L_\mu(M_Z^2)-1-r_{tZ}\Big[B_0^F(\,-s;m_t,m_t)+L_\mu(m_t^2)-2\Big]\\
&-2\left(4-3\frac{m_t^2}{\Delta_{3r}}\right)L_{ab}\left(m_t,m_t,M_Z\right)\Big]\Big\}.
\end{aligned}
\tag{2.67}
$$

In Eq. (2.63) the 'once and twice subtracted' functions B_{d1}^F and B_{d2}^F are met:

$$
\begin{aligned}
B_{d1}^F(\,-m_t^2;m_t,M_Z) &= \frac{1}{r_{tZ}}\Big[B_0^F(\,-m_t^2;m_t,M_Z)+L_\mu(M_Z^2)-1\Big], \qquad (2.68)\\
B_{d2}^F(\,-m_t^2;m_t,M_Z) &= \frac{1}{r_{tZ}^2}\Big[B_0^F(\,-m_t^2;m_t,M_Z)+L_\mu(M_Z^2)-1\\
&\quad -r_{tZ}\left(L_\mu(m_t^2)-L_\mu(M_Z^2)+\frac{1}{2}\right)\Big].
\end{aligned}
$$

They remain finite in the limit $m_t\to 0$.

We note that, for the Z cluster, all the six scalar form factors $F_{L,Q,D}^{\gamma(z)Z}\left(s\right)$ are *separately* gauge-invariant.

2.4.2 Form factors of the H cluster

The diagrams of Fig. 7 contribute to the H cluster,

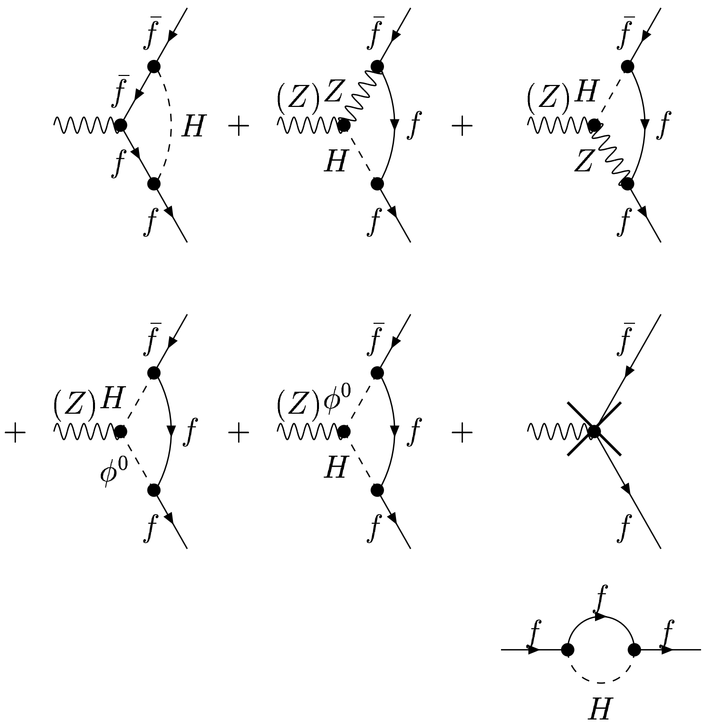

Figure 7: H cluster: the vertices and the counterterm.

Separating UV poles, we have:

$$
\begin{aligned}
F_Q^{\gamma H}(s) &= \mathcal{F}_Q^{\gamma H}(s), \\
F_D^{\gamma H}(s) &= \mathcal{F}_D^{\gamma H}(s), \\
F_L^{zH}(s) &= \frac{1}{4} r_{tw} \frac{1}{\bar{\varepsilon}} + \mathcal{F}_L^{zH}(s), \\
F_Q^{zH}(s) &= \frac{1}{16} \frac{1}{|Q_t|} r_{tw} \frac{1}{s_W^2} \frac{1}{\bar{\varepsilon}} + \mathcal{F}_Q^{zH}(s), \\
F_D^{zH}(s) &= \mathcal{F}_D^{zH}(s),
\end{aligned}
\tag{2.69}
$$

with the finite parts:

$$
\begin{aligned}
\mathcal{F}_Q^{\gamma H}(s) = \; & \frac{1}{8} r_{tw} \Big\{ 8 m_t^2 C_0(-m_t^2, -m_t^2, -s; m_t, M_H, m_t) \\
& + B_0^F(-s; m_t, m_t) + L_\mu(m_t^2) - 2 - B_{d1}^F(-m_t^2; m_t, M_H) \\
& - 2(1 - 4 r_{tH}) M_H^2 B_{0p}(-m_t^2; m_t, M_H) - 2 \frac{M_H^2}{\Delta_{3r}} L_{ab}(m_t, m_t, M_H) \Big\},
\end{aligned}
\tag{2.70}
$$

$$\mathcal{F}_{D}^{\gamma H}(s) = -\frac{Q_t}{2I_t^{(3)}}\frac{r_{tW}}{\Delta_{3r}}\Big\{-6M_H^2 C_0(-m_t^2,-m_t^2,-s;m_t,M_H,m_t)$$
$$+3B_0^F(-s;m_t,m_t)-4B_0^F(-m_t^2;m_t,M_H)-L_\mu(m_t^2)+2$$
$$+B_{d1}^F(-m_t^2;m_t,M_H)+6\frac{M_H^2}{\Delta_{3r}}L_{ab}(m_t,m_t,M_H)\Big\}, \qquad (2.71)$$

$$\mathcal{F}_{L}^{zH}(s) = \frac{1}{4}r_{tW}\Big\{4m_t^2 C_0(-m_t^2,-m_t^2,-s;m_t,M_H,m_t)$$
$$+\Big[4(1-r_{tZ})+(1-r_{HZ})^2R_Z\Big]M_Z^2 C_0(-m_t^2,-m_t^2,-s;M_H,m_t,M_Z)$$
$$+2B_0^F(-s;M_Z,M_H)-\frac{1}{2}B_0^F(-s;m_t,m_t)+\frac{1}{2}L_\mu(m_t^2)$$
$$-\frac{1}{2}B_{d1}^F(-m_t^2;m_t,M_H)-(1-4r_{tH})M_H^2 B_{0p}(-m_t^2;m_t,M_H)+2$$
$$+(1-r_{HZ})R_Z\Big[B_0^F(-m_t^2;M_Z,m_t)-B_0^F(-m_t^2;m_t,M_H)\Big] \qquad (2.72)$$
$$+\frac{M_Z^2}{\Delta_{3r}}\Big[(r_{HZ}-8r_{tZ})L_{ab}(m_t,m_t,M_H)-2(3-r_{HZ}+4r_{tZ})L_{Hi}(m_t,M_H,M_Z)\Big]\Big\},$$

$$\mathcal{F}_{Q}^{zH}(s) = r_{tW}\Big\{m_t^2 C_0(-m_t^2,-m_t^2,-s;m_t,M_H,m_t)$$
$$+\Big[1+(1-r_{HZ})R_Z\Big]M_Z^2 C_0(-m_t^2,-m_t^2,-s;M_H,m_t,M_Z)$$
$$+\frac{1}{8}\Big[B_0^F(-s;m_t,m_t)+L_\mu(m_t^2)-2\Big]$$
$$+R_Z\Big[B_0^F(-m_t^2;M_Z,m_t)-B_0^F(-m_t^2;m_t,M_H)\Big]-\frac{1}{8}B_{d1}^F(-m_t^2;m_t,M_H)$$
$$-\frac{1}{4}(1-4r_{tH})M_H^2 B_{0p}(-m_t^2;m_t,M_H)-\frac{1}{4}\frac{M_H^2}{\Delta_{3r}}L_{ab}(m_t,m_t,M_H)$$
$$+\frac{1}{4}\frac{a_t}{\delta_t}\Big(\Big[4r_{tZ}+(3+r_{HZ})(1-r_{HZ})R_Z\Big]M_Z^2 C_0(-m_t^2,-m_t^2,-s;M_H,m_t,M_Z)$$
$$+B_0^F(-s;m_t,m_t)-2B_0^F(-s;M_Z,M_H)-3$$
$$+(3+r_{HZ})R_Z\Big[B_0^F(-m_t^2;M_Z,m_t)-B_0^F(-m_t^2;m_t,M_H)\Big] \qquad (2.73)$$
$$-2\frac{M_Z^2}{\Delta_{3r}}\Big[(1-4r_{tH})r_{HZ}L_{ab}(m_t,m_t,M_H)-(3-r_{HZ}+4r_{tZ})L_{Hi}(m_t,M_H,M_Z)\Big]\Big)\Big\},$$

$$\mathcal{F}_{D}^{zH}(s) = -\frac{v_t}{2I_t^{(3)}c_W^2}\frac{1}{\Delta_{3r}}\Big\{-3r_{tZ}M_H^2 C_0(-m_t^2,-m_t^2,-s;m_t,M_H,m_t)$$
$$+2\Big[2(r_{HZ}-1)\frac{m_t^2}{s}-r_{HZ}+2r_{tZ}\Big]M_Z^2 C_0(-m_t^2,-m_t^2,-s;M_H,m_t,M_Z)$$

$$
-4\frac{m_t^2}{s}\Big[B_0^F(-m_t^2;M_Z,m_t)-B_0^F(-m_t^2;m_t,M_H)\Big]-2B_0^F(-s;M_Z,M_H)
$$
$$
+2B_0^F(-m_t^2;M_Z,m_t)+\frac{3}{2}r_{tZ}\Big[B_0^F(-s;m_t,m_t)-B_0^F(-m_t^2;m_t,M_H)\Big]
$$
$$
+\frac{1}{2}r_{HZ}\Big[B_0^F(-m_t^2;m_t,M_H)+L_\mu(M_H^2)-1\Big]
$$
$$
-\frac{1}{2}r_{tZ}\Big[B_0^F(-m_t^2;m_t,M_H)+L_\mu(m_t^2)-2\Big]+3r_{tZ}\frac{M_H^2}{\Delta_{3r}}L_{ab}\left(m_t,m_t,M_H\right)\Big\}. \quad (2.74)
$$

Again, the five (one does not exist) scalar form factors in Eq. (2.69) are *separately* gauge-invariant. Note also that UV poles persisting in the scalar form factors of the H cluster cancel exactly the corresponding poles of the Z cluster. In other words, the form factors of the 'neutral sector' cluster $(Z+H)$ are UV finite.

In total, we have 11 separately gauge-invariant *building blocks* that originate from Z and H clusters.

2.4.3 Form factors of the W cluster

Finally, the W cluster is made of the diagrams shown in Fig. 8.

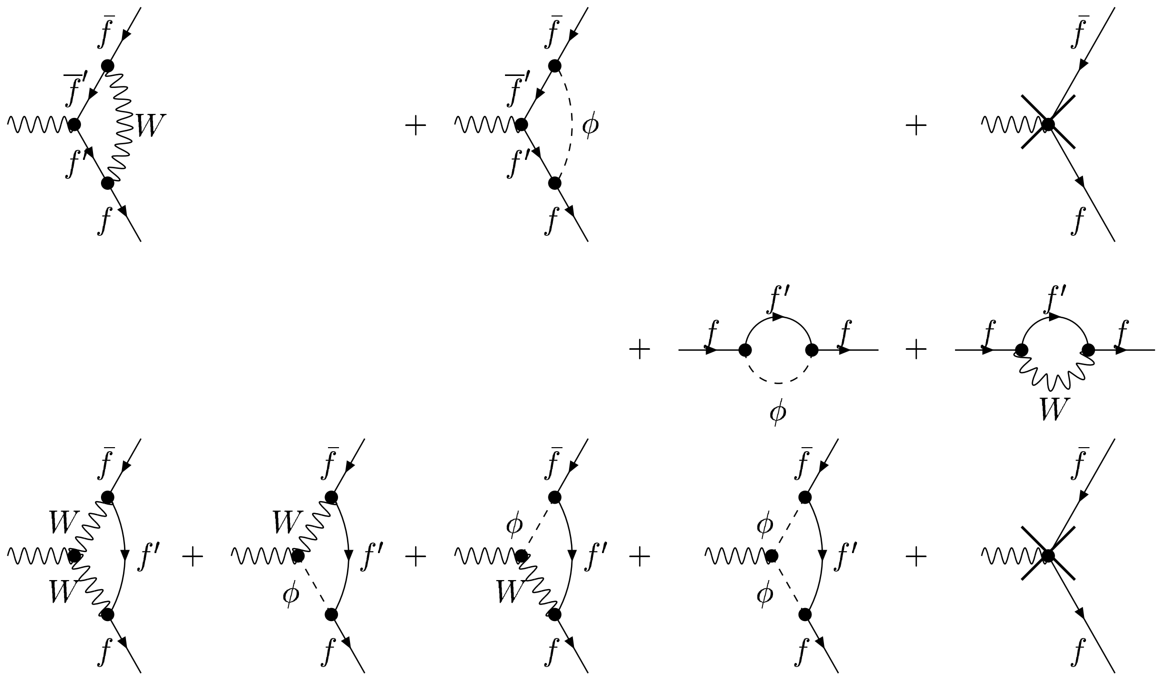

Figure 8: W cluster: the first row shows the abelian diagrams of the cluster, the last row the non-abelian diagrams; the second row shows diagrams that contribute to both counterterm crosses (last diagrams in first and third rows).

In the formulae below, we present contributions to scalar form factors from all the diagrams of the W cluster, not subdividing them into abelian and non-abelian contributions. To some extent two sub-clusters are automatically marked by the type of arguments of C_0 functions and typical coupling constants. Separating poles, we have:

$$\begin{aligned}
\mathcal{F}_{L}^{\gamma W} &= \frac{Q_b}{2I_t^{(3)}}\Biggl\{\Biggl[3+\left(1+r_{tb}^{-}\right)^2+\frac{2}{R_W}\Biggr] M_W^2 C_0(-m_t^2,-m_t^2,-s;m_b,M_W,m_b) \\
&-\frac{1}{2}\left(6+r_{tb}^{-}\right)\Bigl[B_0^F(-s;m_b,m_b)-B_0^F(-m_t^2;m_b,M_W)\Bigr] \\
&+\frac{1}{2}\left(2-r_{tb}^{-}\right)\Bigl[B_{dW}^F(-m_t^2;m_b,M_W)-1\Bigr] \\
&+\Biggl[4-\left(2+r_{tb}^{-}\right)(3+3r_{tW}+r_{bW})\Biggr]\frac{M_W^2}{\Delta_{3r}}L_{ab}(m_t,m_b,M_W)\Biggr\} \\
&-r_{bW}\left(2-r_{tb}^{-}\right)M_W^2 C_0(-m_t^2,-m_t^2,-s;M_W,m_b,M_W) \\
&+\frac{1}{2}\left(6-r_{tb}^{-}\right)\Bigl[B_0^F(-s;M_W,M_W)-B_0^F(-m_t^2;m_b,M_W)\Bigr] \\
&+2B_0^F(-m_t^2;m_b,M_W)+\frac{1}{2}\left(2-3r_{tb}^{-}\right)\Bigl[B_{dW}^F(-m_t^2;m_b,M_W)+1\Bigr] \\
&-\left(4-\Bigl[2+r_{tW}(13+r_{tW})-r_{bW}(1+r_{bW})\Bigr]\frac{M_W^2}{\Delta_{3r}}\right)L_{na}(m_t,m_b,M_W) \\
&-\frac{Q_t}{4I_t^{(3)}}\Bigl(\Delta_{\mathcal{F}_{\rm Im}}-3\Bigr)i\,{\rm Im}B_0^F(-m_t^2;M_W,m_b), \qquad (2.75)
\end{aligned}$$

where

$$\Delta_{\mathcal{F}_{\rm Im}}=(1-r_{bW})\frac{(2+r_{bW})}{r_{tW}}+r_{tW}\,. \qquad (2.76)$$

The last term in Eq. (2.75) is due to a non-cancellation of the imaginary part of the function $B_0^F(-m_t^2;M_W,m_b)$ which appear in real counterterms and complex-valued vertices.

$$\begin{aligned}
\mathcal{F}_{Q}^{\gamma W} &= \frac{r_{tW}}{4Q_t}\Biggl\{Q_b\Biggl[-4M_W^2 C_0(-m_t^2,-m_t^2,-s;m_b,M_W,m_b) \\
&+B_0^F(-s;m_b,m_b)-B_0^F(-m_t^2;m_b,M_W)-1-\frac{2+r_{bW}}{r_{tW}}B_{dW}^F(-m_t^2;m_b,M_W) \\
&-\left(\frac{(1-r_{bW})(2+r_{bW})}{r_{tW}}-1-r_{tW}+2r_{bW}\right)M_W^2 B_{0p}(-m_t^2;m_b,M_W) \\
&+2\left(3+r_{tb}^{-}\right)\frac{M_W^2}{\Delta_{3r}}L_{ab}(m_t,m_b,M_W)\Biggr] \\
&-2I_t^{(3)}\Biggl[2m_b^2 C_0(-m_t^2,-m_t^2,-s;M_W,m_b,M_W) \\
&-B_0^F(-s;M_W,M_W)+B_0^F(-m_t^2;m_b,M_W)-1+\frac{2+r_{bW}}{r_{tW}}B_{dW}^F(-m_t^2;m_b,M_W) \\
&+\left(\frac{2-r_{bW}(1+r_{bW})}{r_{tW}}-1-r_{tW}+2r_{bW}\right)M_W^2 B_{0p}(-m_t^2;m_b,M_W)
\end{aligned}$$

$$+2\Big(7+r_{tb}^{+}\Big)\frac{M_W^2}{\Delta_{3r}}L_{na}\left(m_t,m_b,M_W\right)\Big]\Big\}+\frac{1}{4}\Delta_{\mathcal{F}_{\rm Im}}i\,{\rm Im}B_0^F(-m_t^2;M_W,m_b)\,, \tag{2.77}$$

$$\begin{aligned}
\mathcal{F}_D^{\gamma W} \;=\; & -\frac{1}{\Delta_{3r}}\Bigg\{\frac{Q_b}{2I_t^{(3)}}\Bigg(-2\left[8+r_{tb}^{-2}-6r_{bW}+\frac{2}{R_W}\right]M_W^2C_0(-m_t^2,-m_t^2,-s;m_b,M_W,m_b)\\
& +(10+r_{tW}-3r_{bW})\Big[B_0^F(-s;m_b,m_b)-B_0^F(-m_t^2;m_b,M_W)\Big]\\
& +\Big(2+r_{tb}^{+}\Big)\Big[B_{dW}^F(-m_t^2;m_b,M_W)+1\Big]\\
& +6\Big[(1+r_{tW})(2+r_{tW})-r_{bW}(1+r_{bW})\Big]\frac{M_W^2}{\Delta_{3r}}L_{ab}(m_t,m_b,M_W)\Bigg)\\
& +2\left[\Big(1-r_{tb}^{+}\Big)(2-r_{tW})-r_{bW}\left(1-4r_{bW}-\frac{1}{R_W}\right)\right]\\
& \times M_W^2C_0(-m_t^2,-m_t^2,-s;M_W,m_b,M_W)\\
& +(6-r_{tW}-5r_{bW})\Big[B_0^F(-s;M_W,M_W)-B_0^F(-m_t^2;m_b,M_W)\Big]\\
& +\Big(2+r_{tb}^{+}\Big)\Big[B_{dW}^F(-m_t^2;m_b,M_W)-1\Big]\\
& -6\Big[(1-r_{tW})(2+r_{tW})-r_{bW}(1+2r_{tW}+r_{bW})\Big]\frac{M_W^2}{\Delta_{3r}}L_{na}(m_t,m_b,M_W)\Bigg\},
\end{aligned} \tag{2.78}$$

$$\begin{aligned}
\mathcal{F}_L^{zW} \;=\; & \frac{\sigma_d}{4I_t^{(3)}}\Bigg\{\left[3+\Big(1+r_{tb}^{-}\Big)^2+\frac{2}{R_W}\right]M_W^2C_0(-m_t^2,-m_t^2,-s;m_b,M_W,m_b)\\
& -\frac{1}{2}\Big(6+r_{tb}^{-}\Big)\Big[B_0^F(-s;m_b,m_b)-B_0^F(-m_t^2;m_b,M_W)\Big]\\
& +\frac{1}{2}\Big(2-r_{tb}^{-}\Big)\Big[B_{dW}^F(-m_t^2;m_b,M_W)-1\Big]\\
& +\Big[4-\Big(2+r_{tb}^{-}\Big)(3+3r_{tW}+r_{bW})\Big]\frac{M_W^2}{\Delta_{3r}}L_{ab}(m_t,m_b,M_W)\Bigg\}\\
& +r_{bW}M_W^2C_0(-m_t^2,-m_t^2,-s;m_b,M_W,m_b)\\
& +\frac{1}{4}\Bigg\{r_{tb}^{-}B_0^F(-s;M_W,M_W)-r_{tW}\Big[B_0^F(-m_t^2;m_b,M_W)-1\Big]\\
& +r_{bW}\Big[B_0^F(-s;m_b,m_b)-2\Big]-(2+r_{bW})B_{dW}^F(-m_t^2;m_b,M_W)\\
& -\Big[(1-r_{tW})(2+r_{tW})-r_{bW}(1-2r_{tW}+r_{bW})\Big]M_W^2B_{0p}(-m_t^2;m_b,M_W)\\
& -2r_{bW}\Big(1+r_{tb}^{-}\Big)\frac{M_W^2}{\Delta_{3r}}L_{ab}(m_t,m_b,M_W)\Bigg\}
\end{aligned}$$

$$
\begin{aligned}
&-c_W^2\Biggl\{\Biggl(4\left(1-r_{tW}\right)+\frac{1}{2}r_{bW}\left[4+\frac{s_W^2-c_W^2}{c_W^2}\left(4+r_{tb}^-\right)\right]\Biggr)\\
&\times M_W^2 C_0(-m_t^2,-m_t^2,-s;M_W,m_b,M_W)\\
&+\frac{1}{2}\left(2+r_{tb}^-\right)\left[B_0^F(-m_t^2;M_W,M_W)-B_0^F(-m_t^2;m_b,M_W)\right]\\
&-\frac{1}{2}\left(2-r_{tb}^-\right)\left[B_{dW}^F(-m_t^2;m_b,M_W)+1\right]-2B_0^F(-m_t^2;m_b,M_W)\\
&-\frac{1}{2}\Biggl(4+12r_{tW}-\frac{s_W^2-c_W^2}{c_W^2}r_{tW}\left(7+r_{tW}\right)\\
&-r_{bW}\left[4+\frac{s_W^2-c_W^2}{c_W^2}\left(1-r_{bW}\right)\right]\Biggr)\frac{M_W^2}{\Delta_{3r}}L_{na}\left(m_t,m_b,M_W\right)\Biggr\}\\
&+\frac{1}{8I_t^{(3)}}\Bigl(3\sigma_t-\delta_t\Delta_{\mathcal{F}_{\mathrm{Im}}}\Bigr)i\,\mathrm{Im}B_0^F(-m_t^2;M_W,m_b)\,,
\end{aligned}
\tag{2.79}
$$

$$
\begin{aligned}
\mathcal{F}_Q^{zW} \;=\;& -\frac{r_{tW}}{4}\frac{\sigma_d}{\delta_t}\Biggl\{4M_W^2C_0(-m_t^2,-m_t^2,-s;m_b,M_W,m_b)\\
&-B_0^F(-s;m_b,m_b)+B_0^F(-m_t^2;m_b,M_W)+1-2\left(3+r_{tb}^-\right)\frac{M_W^2}{\Delta_{3r}}L_{ab}\left(m_t,m_b,M_W\right)\Biggr\}\\
&-\frac{1}{4}\left(2+r_{bW}\right)B_{dW}^F(-m_t^2;m_b,M_W)\\
&-\frac{1}{4}\Bigl[\left(1-r_{tW}\right)\left(2+r_{tb}^-\right)+r_{bW}r_{tb}^-\Bigr]M_W^2B_{0p}(-m_t^2;m_b,M_W)\\
&+I_t^{(3)}c_W^2\frac{r_{tW}}{\delta_t}\Biggl\{\frac{s_W^2-c_W^2}{c_W^2}\Biggl(r_{bW}M_W^2C_0(-m_t^2,-m_t^2,-s;M_W,m_b,M_W)\\
&-\frac{1}{2}\Bigl[B_0^F(-s;M_W,M_W)-B_0^F(-m_t^2;m_b,M_W)+1\Bigr]\Biggr)\\
&-\left[8-\frac{s_W^2-c_W^2}{c_W^2}\left(3+r_{tW}+r_{bW}\right)\right]\frac{M_W^2}{\Delta_{3r}}L_{na}\left(m_t,m_b,M_W\right)\Biggr\}\\
&+\frac{1}{4}\Delta_{\mathcal{F}_{\mathrm{Im}}}i\,\mathrm{Im}B_0^F(-m_t^2;M_W,m_b),
\end{aligned}
\tag{2.80}
$$

$$
\begin{aligned}
\mathcal{F}_D^{zW} \;=\;& \frac{1}{\Delta_{3r}}\Biggl\{\frac{v_b+a_b}{2I_t^{(3)}}\Biggl(\left[8+\left(r_{tb}^-\right)^2-6r_{bW}+\frac{2}{R_W}\right]M_W^2C_0(-m_t^2,-m_t^2,-s;m_b,M_W,m_b)\\
&-\frac{1}{2}\left(10+r_{tW}-3r_{bW}\right)\left[B_0^F(-s;m_b,m_b)-B_0^F(-m_t^2;m_b,M_W)\right]\\
&-\frac{1}{2}\left(2+r_{tb}^+\right)\left[B_{dW}^F(-m_t^2;m_b,M_W)+1\right]\\
&-3\Bigl[\left(1+r_{tW}\right)\left(2+r_{tW}\right)-r_{bW}\left(1+r_{bW}\right)\Bigr]\frac{M_W^2}{\Delta_{3r}}L_{ab}\left(m_t,m_b,M_W\right)\Biggr)
\end{aligned}
$$

$$
\begin{aligned}
&+r_{bW}\Bigg(M_W^2 C_0(-m_t^2,-m_t^2,-s;m_b,M_W,m_b)\\
&+\frac{1}{2}\Big[B_0^F(-s;m_b,m_b)-B_0^F(-m_t^2;m_b,M_W)-1\Big]-\frac{1}{2}B_{dW}^F(-m_t^2;m_b,M_W)\\
&-3\left(1+r_{tb}^-\right)\frac{M_W^2}{\Delta_{3r}}L_{ab}\left(m_t,m_b,M_W\right)\Bigg)\\
&-c_W^2\Bigg(\Bigg[4r_{bW}-\frac{s_W^2-c_W^2}{c_W^2}\Big[\left(1-r_{tW}\right)\left(2-r_{tW}\right)-r_{bW}\left(5-r_{tW}-4r_{bW}-\frac{1}{R_Z}\right)\Big]\Bigg]\\
&\times M_W^2 C_0(-m_t^2,-m_t^2,-s;M_W,m_b,M_W)\\
&+\frac{1}{2}\left[4-\frac{s_W^2-c_W^2}{c_W^2}\left(4-r_{tW}-5r_{bW}\right)\right]\Big[B_0^F(-s;M_W,M_W)-B_0^F(-m_t^2;m_b,M_W)\Big]\\
&+\frac{1}{2}\left(4-\frac{s_W^2-c_W^2}{c_W^2}r_{tb}^+\right)\Bigg[B_{dW}^F(-m_t^2;m_b,M_W)-1\\
&-6\left(1-r_{tb}^+\right)\frac{M_W^2}{\Delta_{3r}}L_{na}\left(m_t,m_b,M_W\right)\Bigg]\Bigg)\Bigg\}. \qquad (2.81)
\end{aligned}
$$

Here we introduce more symbols, which were not given in Eq. (2.10):

$$
r_{tb}^{\pm}=r_{tW}\pm r_{bW}\,,\qquad \Delta_{3r}=4m_t^2-s\,. \qquad (2.82)
$$

Furthermore, we used one more 'subtracted' function:

$$
\begin{aligned}
B_{dW}^F(-m_t^2;m_b,M_W) &= \frac{1}{r_{tW}}\Big\{\left(1-r_{bW}\right)\Big[B_0^F(-m_t^2;m_b,M_W)+L_\mu(M_W^2)-1\Big]\\
&\quad -r_{bW}\Big[L_\mu(m_b^2)-L_\mu(M_W^2)\Big]\Big\}, \qquad (2.83)
\end{aligned}
$$

and the three auxiliary functions:

$$
\begin{aligned}
L_{ab}(M_1,M_2,M_3) &= \left(M_3^2+M_1^2-M_2^2\right)C_0(-m_t^2,-m_t^2,-s;M_2,M_3,M_2)\\
&\quad -B_0^F(-s;M_2,M_2)+B_0^F(-m_t^2;M_2,M_3), \qquad (2.84)\\
L_{na}(M_1,M_2,M_3) &= \left(M_3^2-M_1^2-M_2^2\right)C_0(-m_t^2,-m_t^2,-s;M_3,M_2,M_3)\\
&\quad +B_0^F(-s;M_3,M_3)-B_0^F(-m_t^2;M_3,M_2), \qquad (2.85)\\
L_{Hi}(M_1,M_2,M_3) &= \left[\frac{1}{2}\left(M_2^2+M_3^2\right)-2M_1^2\right]C_0(-m_t^2,-m_t^2,-s;M_2,M_1,M_3) \qquad (2.86)\\
&\quad +B_0^F(-s;M_3,M_2)-\frac{1}{2}B_0^F(-m_t^2;M_1,M_2)-\frac{1}{2}B_0^F(-m_t^2;M_3,M_1).
\end{aligned}
$$

Four scalar form factors, $\mathcal{F}_{Q,D}^{\gamma(z)W}$, as follows from calculations, are both gauge-invariant and finite, thus enlarging the number of gauge-invariant *building blocks* to 15. On the contrary, two form factors, $\mathcal{F}_L^{\gamma(z)W}$, are neither gauge-invariant nor finite. Gauge dependence on ξ, as well as UV poles, of L form factors cancel in the sum with the WW box and the self-energy contributions.

2.5 Library of scalar form factors for electron vertex

Besides Btt clusters, we need also Bee clusters, which can, in principle, be taken from [6] or derived from the Btt case in the $m_t \to 0$ limit. Here we simply list the results:

$$
\begin{aligned}
\mathcal{F}_{L}^{\gamma ee}(s,t) &= -\frac{2}{c_W^2} Q_e v_e a_e \mathcal{F}^{Z,e}(s) + \mathcal{F}^{Wna,e}(s), \\
\mathcal{F}_{Q}^{\gamma ee}(s,t) &= \frac{1}{4c_W^2}\delta_e^2 \mathcal{F}^{Z,e}(s), \\
\mathcal{F}_{L}^{zee}(s,t) &= -\frac{1}{2c_W^2} A_e \mathcal{F}^{Z,e}(s) + \mathcal{F}^{W,e}(s), \\
\mathcal{F}_{Q}^{zee}(s) &= \frac{1}{4c_W^2}\delta_e^2 \mathcal{F}^{Z,e}(s),
\end{aligned}
\tag{2.87}
$$

with

$$
\mathcal{F}^{W,e}(s) = -\mathcal{F}^{Wab,e}(s) + c_W^2 \mathcal{F}^{Wna,e}(s). \tag{2.88}
$$

In Eq. (2.87) we use three more auxiliary functions:

$$
\begin{aligned}
\mathcal{F}^{Z,e} \equiv \mathcal{F}^{Zab,e} &= 2\frac{(1+R_Z)^2}{R_Z} M_Z^2 C_0(0,0,-s;0,M_Z,0) - 3\left[B_0^F(-s;0,0) + L_\mu(M_Z^2)\right] \\
&\quad + \frac{5}{2} - 2R_Z\left[B_0^F(-s;0,0) + L_\mu(M_Z^2) - 1\right],
\end{aligned}
\tag{2.89}
$$

$$
\begin{aligned}
\mathcal{F}^{Wna,e} &= -2R_W\left[M_W^2 C_0(0,0,-s;M_W,0,M_W) + B_0^F(-s;M_W,M_W) + L_\mu(M_W^2) - 1\right] \\
&\quad -4M_W^2 C_0(0,0,-s;M_W,0,M_W) - B_0^F(-s;M_W,M_W) - 3L_\mu(M_W^2) + \frac{9}{2},
\end{aligned}
\tag{2.90}
$$

$$
\begin{aligned}
\mathcal{F}^{Wab,e} &= \sigma_\nu\Biggl\{\frac{(1+R_W)^2}{R_W} M_W^2 C_0(0,0,-s;0,M_W,0) - \frac{3}{2}\left[B_0^F(-s;0,0) + L_\mu(M_W^2)\right] \\
&\quad + \frac{5}{4} - R_W\left[B_0^F(-s;0,0) + L_\mu(M_W^2) - 1\right]\Biggr\}.
\end{aligned}
\tag{2.91}
$$

2.6 The WW box

There is only one, *crossed*, WW diagram contributing to our process, see Fig. 9.

Here we give the contribution of this diagram to the scalar form factor LL:

$$
\left(\mathcal{B}^{WW}\right)^c = (2\pi)^4 i \frac{g^4}{16\pi^2}\frac{1}{s}\gamma_\mu\gamma_+ \otimes \gamma_\mu\gamma_+ \mathcal{F}_{LL}^{WW}(s,u), \tag{2.92}
$$

where

$$
\begin{aligned}
\mathcal{F}_{LL}^{WW}(s,u) &= \frac{s}{8}\Bigl[-\left(u-m_b^2\right) D_0(0,0,-m_t^2,-m_t^2,-s,-u;M_W,0,M_W,m_b) \\
&\quad + C_0(-m_t^2,-m_t^2,-s;M_W,0,M_W) + C_0(0,0,-s;M_W,0,M_W)\Bigr],
\end{aligned}
\tag{2.93}
$$

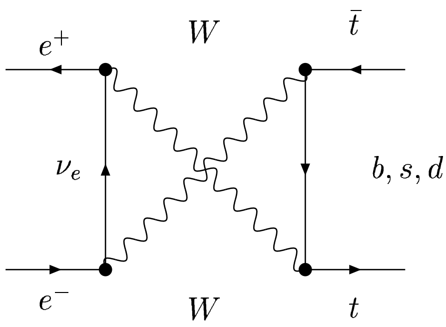

Figure 9: Crossed WW box.

with s, t, and u being the usual Mandelstamm variables satisfying

$$s + t + u = 2m_t^2 \,. \tag{2.94}$$

2.7 The ZZ box

There are four ZZ diagrams, which form a gauge-invariant and UV finite subset. Its contribution is originally presented in terms of six structures $(L,R) \otimes (L,R,D)$ (i.e. here we used initially the L,R,D basis):

$$\begin{aligned}\left(\mathcal{B}^{ZZ}\right)^{d+c} = \; & \frac{1}{32}\frac{g^4}{c_W^4}\frac{1}{s}\Big[\left[\gamma_\mu\gamma_+ \otimes \gamma_\mu\gamma_+\right]\mathcal{F}^{ZZ}_{LL}(s,t,u) + \left[\gamma_\mu\gamma_+ \otimes \gamma_\mu\gamma_-\right]\mathcal{F}^{ZZ}_{LR}(s,t,u) \\ & + \left[\gamma_\mu\gamma_- \otimes \gamma_\mu\gamma_+\right]\mathcal{F}^{ZZ}_{RL}(s,t,u) + \left[\gamma_\mu\gamma_- \otimes \gamma_\mu\gamma_-\right]\mathcal{F}^{ZZ}_{RR}(s,t,u) \\ & + \left[\gamma_\mu\gamma_+ \otimes (-im_t I D_\mu)\right]\mathcal{F}^{ZZ}_{LD}(s,t,u) + \left[\gamma_\mu\gamma_- \otimes (-im_t I D_\mu)\right]\mathcal{F}^{ZZ}_{RD}(s,t,u)\Big].\end{aligned} \tag{2.95}$$

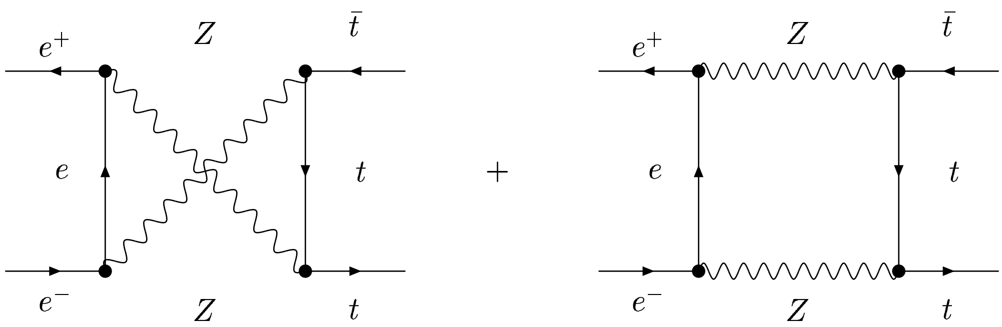

Figure 10: Crossed and direct ZZ boxes.

Moreover, we used three auxiliary functions $\mathcal{F}, \mathcal{H}, \mathcal{G}$:

$$\mathcal{F}^{ZZ}_{LD}(s,t,u) = \mathcal{F}(\sigma_e, \sigma_t, \delta_t, s, t) - \mathcal{F}(\sigma_e, \delta_t, \sigma_t, s, u)\,,$$

$$
\begin{aligned}
\mathcal{F}^{ZZ}_{RD}(s,t,u) &= \mathcal{F}(\delta_e,\delta_t,\sigma_t,s,t)-\mathcal{F}(\delta_e,\sigma_t,\delta_t,s,u)\,,\\
\mathcal{F}^{ZZ}_{LR}(s,t,u) &= \mathcal{H}(\sigma_e,\sigma_t,\delta_t,s,t)-\mathcal{G}(\sigma_e,\delta_t,\sigma_t,s,u)\,,\\
\mathcal{F}^{ZZ}_{RL}(s,t,u) &= \mathcal{H}(\delta_e,\delta_t,\sigma_t,s,t)-\mathcal{G}(\delta_e,\sigma_t,\delta_t,s,u)\,,\\
\mathcal{F}^{ZZ}_{LL}(s,t,u) &= \mathcal{G}(\sigma_e,\sigma_t,\delta_t,s,t)-\mathcal{H}(\sigma_e,\delta_t,\sigma_t,s,u)\,,\\
\mathcal{F}^{ZZ}_{RR}(s,t,u) &= \mathcal{G}(\delta_e,\delta_t,\sigma_t,s,t)-\mathcal{H}(\delta_e,\sigma_t,\delta_t,s,u)\,.
\end{aligned}
\tag{2.96}
$$

Separating out Z fermion coupling constants and some common factors, we introduce more auxiliary functions. For $\mathcal{F}(\sigma_e,\sigma_t,\delta_t,s,t)$ defined as

$$
\mathcal{F}(\sigma_e,\sigma_t,\delta_t,s,t) = \frac{s}{\Delta_{4r}}\Big[\sigma_e^2\sigma_t^2\mathcal{F}_1(s,t)+\sigma_e^2\sigma_t\delta_t\mathcal{F}_2(s,t)\Big],
\tag{2.97}
$$

there are two

$$
\begin{aligned}
\mathcal{F}_1(s,t) = &\left(t_+M_Z^2+t_-^2+\left[\left(-s_z+2M_Z^2\right)t_-^2+4tM_Z^4\right]\frac{t_-}{\Delta_{4r}}\right)\\
&\times D_0(0,0,-m_t^2,-m_t^2,-s,-t;M_Z,0,M_Z,m_t)\\
&-\left[m_t^2-M_Z^2-\frac{t_-\left(t_-t+2M_Z^2t_+\right)+sm_t^4}{\Delta_{4r}}+\frac{2t_+\left(M_Z^2-2m_t^2\right)}{\Delta_{3r}}\right]\\
&\times C_0(-m_t^2,-m_t^2,s;M_Z,m_t,M_Z)\\
&-2\left[t\left(1+\frac{M_Z^2}{t_-}\right)+\frac{t^3+2tt_-M_Z^2-m_t^2\left(3tt_-+m_t^4\right)}{\Delta_{4r}}\right]C_0(0,-m_t^2,t;0,M_Z,m_t)\\
&-\left[M_Z^2-m_t^2+\frac{\left(t-2t_--2M_Z^2\right)t_-^2+sm_t^4}{\Delta_{4r}}\right]C_0(0,0,s;M_Z,0,M_Z)\\
&-\left(1+\frac{s+2t_-}{\Delta_{3r}}\right)\Big[B_0(-s;M_Z,M_Z)-B_0(-m_t^2;M_Z,m_t)\Big]\\
&+\frac{2t}{t_-}\Big[B_0(t;m_t,0)-B_0(-m_t^2;M_Z,m_t)\Big]\Bigg\},
\end{aligned}
\tag{2.98}
$$

and

$$
\begin{aligned}
\mathcal{F}_2(s,t) = &-\left(t_-^2+2M_Z^2t\right)D_0(0,0,-m_t^2,-m_t^2,-s,-t;M_Z,0,M_Z,m_t)\\
&-t_+C_0(-m_t^2,-m_t^2,s;M_Z,m_t,M_Z)\\
&+2tC_0(0,-m_t^2,t;0,M_Z,m_t)-t_-C_0(0,0,s;M_Z,0,M_Z).
\end{aligned}
\tag{2.99}
$$

For $\mathcal{H}$ written out as

$$
\mathcal{H}(\sigma_e,\sigma_t,\delta_t,s,t) = \frac{m_t^2s}{\Delta_{4r}}\Big[\sigma_e^2\sigma_t^2\mathcal{H}_1(s,t)+\sigma_e^2\sigma_t\delta_t\mathcal{H}_2(s,t)\Big]+\sigma_e^2\delta_t^2\mathcal{H}_3(s,t)\,,
\tag{2.100}
$$

we need three auxiliary subfunctions:

$$
\mathcal{H}_1(s,t) = \left[\frac{st_-}{2}-(t_-+M_Z^2)^2-2M_Z^2t-\frac{s_z^2t_-t_+}{2\Delta_{4r}}\right]
$$

$$
\begin{aligned}
& \times D_0(0,0,-m_t^2,-m_t^2,-s,-t;M_Z,0,M_Z,m_t) \\
& -\left(t_+ - \frac{s_z\left[t_+^2+\Delta_{3r}m_t^2\right]}{2\Delta_{4r}}\right)C_0(-m_t^2,-m_t^2,s;M_Z,m_t,M_Z) \\
& +\left(2t+t_- + \frac{2M_Z^2 t}{t_-} - \frac{s_z t_- t_+}{\Delta_{4r}}\right)C_0(0,0,s;M_Z,0,M_Z) \\
& -\left[t_- + \frac{s_z\left(sm_t^2 - t_-^2\right)}{2\Delta_{4r}}\right]C_0(0,-m_t^2,t;0,M_Z,m_t) \qquad (2.101) \\
& -2\frac{m_t^2}{t_-}\left(B_0(t;m_t,0) - B_0(-m_t^2;M_Z,m_t)\right) - B_0(t;m_t,0) + B_0(s;M_Z,M_Z),
\end{aligned}
$$

$$
\begin{aligned}
\mathcal{H}_2(s,t) \;=\; & \left[t_-(s+t_-) + 2m_t^2M_Z^2\right]D_0(0,0,-m_t^2,-m_t^2,-s,-t;M_Z,0,M_Z,m_t) \\
& -\left(s+t_- - 2m_t^2\right)C_0(-m_t^2,-m_t^2,s;M_Z,m_t,M_Z) \qquad (2.102) \\
& -2m_t^2C_0(-m_t^2,-m_t^2,s;0,M_Z,m_t) + (s+t_-)\,C_0(0,0,s;M_Z,0,M_Z),
\end{aligned}
$$

and

$$
\begin{aligned}
\mathcal{H}_3(s,t) \;=\; & -s\Big[t_-D_0(0,0,-m_t^2,-m_t^2,-s,-t;M_Z,0,M_Z,m_t) \\
& +C_0(-m_t^2,-m_t^2,s;M_Z,m_t,M_Z) + C_0(0,-m_t^2,t;M_Z,0,M_Z)\Big]. \qquad (2.103)
\end{aligned}
$$

Finally, $\mathcal{G}$ also, defined as follows:

$$
\mathcal{G}(\sigma_e,\sigma_t,\delta_t,s,t) = \frac{s}{\Delta_{4r}}\left[\sigma_e^2\sigma_t^2\mathcal{G}_1(s,t) + \sigma_e^2\sigma_t\delta_t\mathcal{G}_2(s,t)\right], \qquad (2.104)
$$

needs only two additional functions:

$$
\begin{aligned}
\mathcal{G}_1(s,t) \;=\; & -\left[t_-t_+\left(2M_Z^2 + \frac{s_z^2 t}{2\Delta_{4r}}\right) - t_-\left(\frac{sm_t^2}{2} - t_-t\right) + tM_Z^2\left(2m_t^2 - M_Z^2\right)\right] \\
& \times D_0(0,0,-m_t^2,-m_t^2,-s,-t;M_Z,0,M_Z,m_t) \\
& +\left[t_+t + \frac{s_z}{2}\left(t - \frac{t_-t_+^2}{\Delta_{4r}}\right)\right]C_0(-m_t^2,-m_t^2,s;M_Z,m_t,M_Z) \\
& -\left[t_+(t+t_-) + 2M_Z^2m_t^2\frac{t}{t_-} - \frac{t_+t_-ts_z}{\Delta_{4r}}\right]C_0(0,-m_t^2,-t;0,M_Z,m_t) \\
& -\left[t_-t + \frac{s_z}{2}\left(t - \frac{t_+t_-^2}{\Delta_{4r}}\right)\right]C_0(0,0,s;M_Z,0,M_Z) \\
& +2m_t^2\left(1 + \frac{m_t^2}{t_-}\right)\left[B_0(t;m_t,0) - B_0(-m_t^2;M_Z,m_t)\right] \\
& -t\Big[B_0(s;M_Z,M_Z) - B_0(t;m_t,0)\Big], \qquad (2.105)
\end{aligned}
$$

and

$$
\begin{aligned}
\mathcal{G}_2(s,t) &= m_t^2\Big[(t_-^2+2M_Z^2t)D_0(0,0,-m_t^2,-m_t^2,-s,-t;M_Z,0,M_Z,m_t) \\
&\quad +t_+C_0(-m_t^2,-m_t^2,s;M_Z,m_t,M_Z)-2tC_0(0,-m_t^2,t;0,M_Z,m_t) \\
&\quad +t_-C_0(0,0,s;M_Z,0,M_Z)\Big]. \qquad (2.106)
\end{aligned}
$$

In this section we used the notation:

$$\Delta_{4r} = -tu+m_t^4\,; \qquad (2.107)$$

together with Δ_{3r} of Eq. (2.82), this denotes remnants of Gram determinants that remained after cancellation of factors s and 4, leading to a simplification of the expressions.

2.7.1 Transition to the L, Q, D basis

Since the ZZ box contribution is given in the L, R, D basis, while all the rest is in the L, Q, D basis, we should transfer one of them to a chosen basis. At this phase of the calculations there is not much difference which basis is chosen. For definiteness we choose the L, Q, D basis and transfer the ZZ box contribution to it.The transition formulae are simple:

$$
\begin{aligned}
\tilde{\mathcal{F}}^{ZZ}_{LL}(s,t,u) &= \mathcal{F}^{ZZ}_{LL}(s,t,u)+\mathcal{F}^{ZZ}_{RR}(s,t,u)-\mathcal{F}^{ZZ}_{LR}(s,t,u)-\mathcal{F}^{ZZ}_{RL}(s,t,u)\,, \\
\tilde{\mathcal{F}}^{ZZ}_{QL}(s,t,u) &= 2\Big[\mathcal{F}^{ZZ}_{RL}(s,t,u)-\mathcal{F}^{ZZ}_{RR}(s,t,u)\Big], \\
\tilde{\mathcal{F}}^{ZZ}_{LQ}(s,t,u) &= 2\Big[\mathcal{F}^{ZZ}_{LR}(s,t,u)-\mathcal{F}^{ZZ}_{RR}(s,t,u)\Big], \\
\tilde{\mathcal{F}}^{ZZ}_{QQ}(s,t,u) &= 4\mathcal{F}^{ZZ}_{RR}(s,t,u)\,, \\
\tilde{\mathcal{F}}^{ZZ}_{LD}(s,t,u) &= \mathcal{F}^{ZZ}_{LD}(s,t,u)-\mathcal{F}^{ZZ}_{RD}(s,t,u)\,, \\
\tilde{\mathcal{F}}^{ZZ}_{QD}(s,t,u) &= 2\mathcal{F}^{ZZ}_{RD}(s,t,u)\,. \qquad (2.108)
\end{aligned}
$$

3 Scalar form factors for electroweak amplitude

Having all the building blocks, it is time to construct *complete* electroweak scalar form factors.

3.1 Vertices scalar form factors

We begin with two vertex contributions:

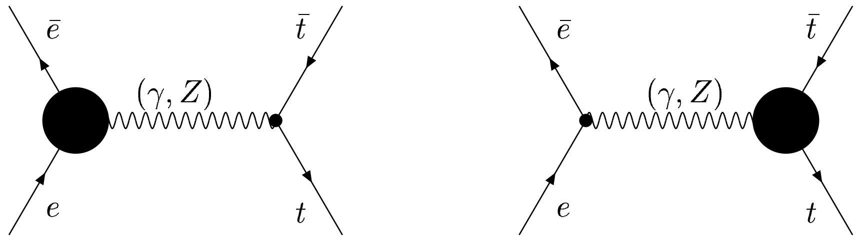

Figure 11: *Electron (a) and final fermion (b) vertices in $e\bar{e} \to (\gamma, Z) \to f\bar{f}$.*

In the same way as described in [6], we reduce two vertex contributions to our six form factors:

$$
\begin{aligned}
F_{LL}(s) &= F_L^{zee}(s) + F_L^{ztt}(s) - 4c_W^2\Delta(M_W), \\
F_{QL}(s) &= F_Q^{zee}(s) + F_L^{ztt}(s) - 2c_W^2\Delta(M_W) + k\left[F_L^{\gamma tt}(s) - 2\Delta(M_W)\right], \\
F_{LQ}(s) &= F_L^{zee}(s) - 2c_W^2\Delta(M_W) + F_Q^{ztt}(s) + k\left[F_L^{\gamma ee}(s) - 2\Delta(M_W)\right], \\
F_{QQ}(s) &= F_Q^{zee}(s) + F_Q^{ztt}(s) - \frac{k}{s_W^2}\left[F_Q^{\gamma ee}(s) + F_Q^{\gamma tt}(s)\right], \\
F_{LD}(s) &= F_D^{ztt}(s), \\
F_{QD}(s) &= F_D^{ztt}(s) + kF_D^{\gamma tt}(s),
\end{aligned}
\tag{3.109}
$$

where

$$
k = c_W^2\left(R_Z - 1\right). \tag{3.110}
$$

With the term containing $\Delta(M_W)$,

$$
\Delta(M_W) = \frac{1}{\bar{\varepsilon}} - \ln\frac{M_W^2}{\mu^2}, \tag{3.111}
$$

we explicitly show the contribution of the so-called *special* vertices [21]. Note that they accompany every L form factor. The poles $1/\bar{\varepsilon}$ originating from special vertices will be canceled in the sum of all contributions, including self-energies and boxes.

3.2 Bosonic self-energies and bosonic counterterms

The contributions to form factors from bosonic self-energy diagrams and counterterms, originating from bosonic self-energy diagrams, come from four classes of diagrams; their sum is depicted by a black circle in Fig. 12.

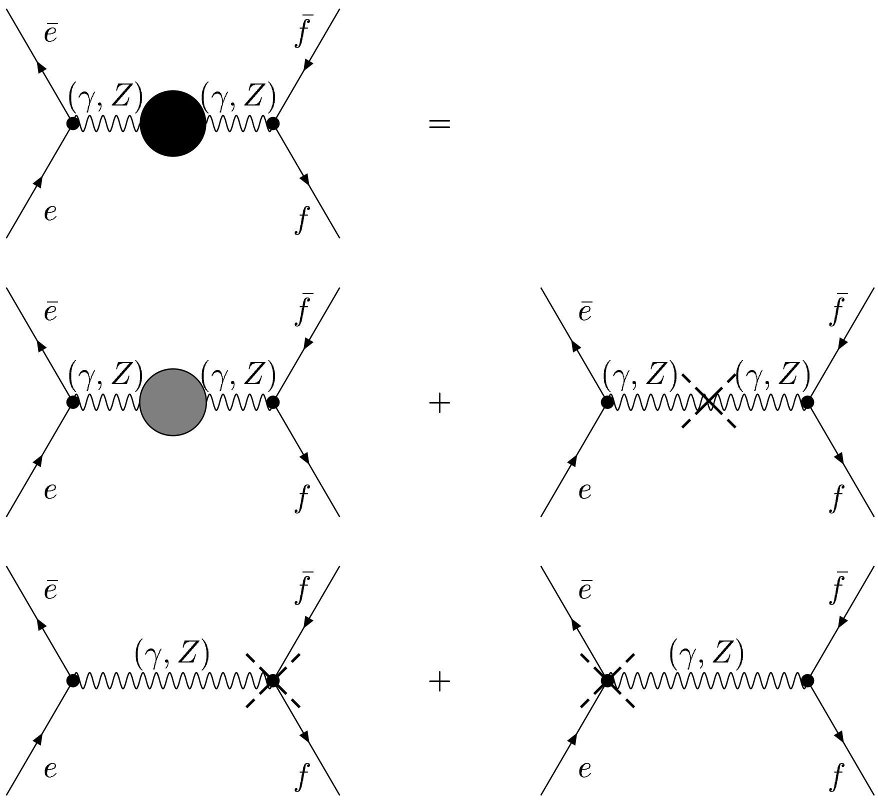

Figure 12: *Bosonic self-energies and bosonic counterterms for* $e\bar{e} \to (Z,\gamma) \to f\bar{f}$.

The contribution of these diagrams to the four scalar form factors is derived straightforwardly [7], [6]:

$$F^{ct}_{LL}(s) = \mathcal{D}_{Z}(s) - s^2_W \Pi_{\gamma\gamma}(0) + \frac{c^2_W - s^2_W}{s^2_W}\left(\Delta\rho + \Delta\bar{\rho}^{\rm bos}\right), \tag{3.112}$$

$$F^{ct}_{QL(LQ)}(s) = \mathcal{D}_{Z}(s) - \left(\Pi_{Z\gamma}(s) + \bar{\Pi}^{\rm bos}_{Z\gamma}(s)\right) - s^2_W \Pi_{\gamma\gamma}(0) - \left(\Delta\rho + \Delta\bar{\rho}^{\rm bos}\right), \tag{3.113}$$

$$\begin{aligned} F^{ct,\rm bos}_{QQ}(s) = {} & \mathcal{D}^{\rm bos}_{Z}(s) - 2\left(\Pi^{\rm bos}_{Z\gamma}(s) + \bar{\Pi}^{\rm bos}_{Z\gamma}(s)\right) + k\Big[\Pi^{\rm bos}_{\gamma\gamma}(s) - \Pi^{\rm bos}_{\gamma\gamma}(0)\Big] \\ & - s^2_W \Pi^{\rm bos}_{\gamma\gamma}(0) - \frac{1}{s^2_W}\left(\Delta\rho^{\rm bos} + \Delta\bar{\rho}^{\rm bos}\right), \end{aligned} \tag{3.114}$$

$$F^{ct,\rm fer}_{QQ}(s) = \mathcal{D}^{\rm fer}_{Z}(s) - 2\Pi^{\rm fer}_{Z\gamma}(s) - s^2_W \Pi^{\rm fer}_{\gamma\gamma}(0) - \frac{1}{s^2_W}\Delta\rho^{\rm fer}. \tag{3.115}$$

We note that the term $k[\Pi^{\rm fer}_{\gamma\gamma}(s) - \Pi^{\rm fer}_{Z\gamma}(s)]$ is conventionally extracted from $F^{ct,{\rm fer}}_{QQ}(s)$. This contribution is shifted to $A^{\rm IBA}_{\gamma}$, Eq. (1.8).

In Eqs. (3.112)–(3.115) $\Delta\bar{\rho}^{\rm bos}$ and $\bar{\Pi}^{\rm bos}_{Z\gamma}(s)$ stand for shifts of bosonic self-energies. They have the same origin as special vertices and they are equal to:

$$\begin{aligned}
\Delta\bar{\rho}^{\rm bos} &= 4s^2_W\Delta(M_W), &(3.116)\\
\bar{\Pi}^{\rm bos}_{Z\gamma}(s) &= -2R_W\Delta(M_W), &(3.117)
\end{aligned}$$

see Eqs. (6.137) and (6.139) of [7]. These poles also cancel in the sum of all contributions.

3.3 Complete scalar form factors of the one-loop amplitude

Adding all contributions together, we observe the cancellation of all poles. The ultraviolet-finite results for six scalar form factors are:

$$\begin{aligned}
F_{LL}(s,t,u) &= \mathcal{F}^{zee}_{L}(s) + \mathcal{F}^{ztt}_{L}(s) + \mathcal{F}^{ct}_{LL}(s) + k^{WW}\,\mathcal{F}^{WW}_{LL}(s,u) + k^{ZZ}\,\mathcal{F}^{ZZ}_{LL}(s,t,u)\,,\\
F_{QL}(s,t,u) &= \mathcal{F}^{zee}_{Q}(s) + \mathcal{F}^{ztt}_{L}(s) + k\,\mathcal{F}^{\gamma tt}_{L}(s) + \mathcal{F}^{ct}_{QL}(s) + k^{ZZ}\,\mathcal{F}^{ZZ}_{QL}(s,t,u)\,,\\
F_{LQ}(s,t,u) &= \mathcal{F}^{zee}_{L}(s) + \mathcal{F}^{ztt}_{Q}(s) + k\,\mathcal{F}^{\gamma ee}_{L}(s) + \mathcal{F}^{ct}_{LQ}(s) + k^{ZZ}\,\mathcal{F}^{ZZ}_{LQ}(s,t,u)\,,\\
F_{QQ}(s,t,u) &= \mathcal{F}^{zee}_{Q}(s) + \mathcal{F}^{ztt}_{Q}(s) - \frac{k}{s^2_W}\left[\mathcal{F}^{\gamma ee}_{Q}(s) + \mathcal{F}^{\gamma tt}_{Q}(s)\right] + \mathcal{F}^{ct}_{QQ}(s) + k^{ZZ}\,\mathcal{F}^{ZZ}_{QQ}(s,t,u)\,,\\
F_{LD}(s,t,u) &= \mathcal{F}^{ztt}_{D}(s) + k^{ZZ}\,\mathcal{F}^{ZZ}_{LD}(s,t,u)\,,\\
F_{QD}(s,t,u) &= \mathcal{F}^{ztt}_{D}(s) + k\,\mathcal{F}^{\gamma tt}_{D}(s) + k^{ZZ}\,\mathcal{F}^{ZZ}_{QD}(s,t,u)\,, &(3.118)
\end{aligned}$$

where

$$k^{WW} = 16k\,, \tag{3.119}$$

$$k^{ZZ} = \frac{(R_Z - 1)}{2c^2_W}\,. \tag{3.120}$$

In Eq. (3.118), the quantities $\mathcal{F}^{ct}_{AB}(s)$ denote finite parts of the counterterm contributions, see Eqs. (3.112)–(3.115).

The formulae of Sections 2 and 3 put together present the one-loop core of the `eeffLib` code.

4 Improved Born Approximation cross-section

In this section we give the improved Born approximation (IBA) differential in the scattering angle cross-section. It is derived by simple squaring the $(\gamma + Z)$ exchange IBA amplitude, Eqs. (1.8)–(1.10), and accounting for proper normalization factors. We simply give the result:

$$\frac{d\sigma^{\rm IBA}}{d\cos\vartheta} = \frac{\pi\alpha^2}{s^3}\beta_t N_c(\sigma^{IBA}_{\gamma\gamma} + \sigma^{IBA}_{\gamma Z} + \sigma^{IBA}_{ZZ}), \tag{4.121}$$

where $\beta_t = \sqrt{1 - 4m_t^2/s}$ and

$$\begin{aligned}
\sigma^{IBA}_{\gamma\gamma} &= Q_t^2\left(s^2 + 2st + 2t_-^2\right)\left|\alpha\left(s\right)\right|^2, \\
\sigma^{IBA}_{\gamma Z} &= 2Q_t{\rm Re}\Big\{\chi\Big(2\left[\left(s+t_-\right)^2 + sm_t^2\right]\tilde{F}_{LL}\left(s,t,u\right) \\
&\quad + \left(s^2 + 2st + 2t_-^2\right)\left[\tilde{F}_{QL}\left(s,t,u\right) + \tilde{F}_{LQ}\left(s,t,u\right) + \tilde{F}_{QQ}\left(s,t,u\right)\right] \\
&\quad -4m_t^2\left(st + t_-^2\right)\left[\tilde{F}_{LD}\left(s,t,u\right) + \tilde{F}_{QD}\left(s,t,u\right)\right]\Big)\alpha^*\left(s\right)\Big\}, \\
\sigma^{IBA}_{ZZ} &= |\chi|^2{\rm Re}\Big\{8\left(s+t_-\right)^2\left[\left|\tilde{F}_{LL}\left(s,t,u\right)\right|^2 + \tilde{F}_{LL}\left(s,t,u\right)\tilde{F}^*_{QL}\left(s,t,u\right)\right] \\
&\quad +2\left[\left(s+t_-\right)^2 + t_-^2\right]\left|\tilde{F}_{QL}\left(s,t,u\right)\right|^2 \\
&\quad +4\left[\left(s+t_-\right)^2 + sm_t^2\right]\Big[2\tilde{F}_{LL}\left(s,t,u\right)\tilde{F}^*_{LQ}\left(s,t,u\right) \\
&\quad +\tilde{F}_{LL}\left(s,t,u\right)\tilde{F}^*_{QQ}\left(s,t,u\right) + \tilde{F}_{QL}\left(s,t,u\right)\tilde{F}^*_{LQ}\left(s,t,u\right)\Big] \\
&\quad +\left[s^2 + 2\left(st + t_-^2\right)\right]\Big[2\left|\tilde{F}_{LQ}\left(s,t,u\right)\right|^2 + \left|\tilde{F}_{QQ}\left(s,t,u\right)\right|^2 \\
&\quad +2\Big(\tilde{F}_{QL}\left(s,t,u\right) + \tilde{F}_{LQ}\left(s,t,u\right)\Big)\tilde{F}^*_{QQ}\left(s,t,u\right)\Big] \\
&\quad -8m_t^2\left(st + t_-^2\right)\Big[\Big(2\tilde{F}_{LD}\left(s,t,u\right) + \tilde{F}_{QD}\left(s,t,u\right)\Big)\tilde{F}^*_{LL}\left(s,t,u\right) \\
&\quad +\Big(\tilde{F}_{LD}\left(s,t,u\right) + \tilde{F}_{QD}\left(s,t,u\right)\Big)\tilde{F}^*_{QL}\left(s,t,u\right) \\
&\quad +\Big(2\tilde{F}_{LD}\left(s,t,u\right) + \tilde{F}_{QD}\left(s,t,u\right)\Big)\tilde{F}^*_{LQ}\left(s,t,u\right) \\
&\quad +\Big(\tilde{F}_{LD}\left(s,t,u\right) + \tilde{F}_{QD}\left(s,t,u\right)\Big)\tilde{F}^*_{QQ}\left(s,t,u\right)\Big] \\
&\quad -2m_t^2\left(st + t_-^2\right)\Delta_{3r}\Big[2\left|\tilde{F}_{LD}\left(s,t,u\right)\right|^2 \\
&\quad +2\tilde{F}_{LD}\left(s,t,u\right)\tilde{F}^*_{QD}\left(s,t,u\right) + \left|\tilde{F}_{QD}\left(s,t,u\right)\right|^2\Big]\Big\}.
\end{aligned} \tag{4.122}$$

5 Numerical results and discussion

All the formulae derived in this article are realized in a FORTRAN code with a tentative name eeffLib. All the numbers are produced with December 2000 version of the code [18]. In this section we present several examples of numerical results.

We will show several examples of comparison with ZFITTER v6.30 [19]. In the present realization, eeffLib does not calculate M_W from μ decay and does not precompute either Sirlin's parameter Δr or total Z width, which enters the Z boson propagator. For this reason, the three parameters: M_W , Δr , Γ_Z were being taken from ZFITTER and used as INPUT for eeffLib. Moreover, present eeffLib is a purely one-loop code, while in ZFITTER it was not foreseen to access one-loop form factors with users flags. To accomplish the goals of comparison at the one-loop level, we had to modify a little the DIZET electroweak library. The most important change was an addition to the SUBROUTINE ROKANC:

```
*
* For eett
*
      FLL=(XROK(1)-1D0+DR )*R1/AL4PI
      FQL=FLL+(XROK(2)-1D0)*R1/AL4PI
      FLQ=FLL+(XROK(3)-1D0)*R1/AL4PI
      FQQ=FLL+(XROK(4)-1D0)*R1/AL4PI
```

with the aid of which we reconstruct four form factors from ZFITTER's effective couplings ρ and κ's (F_{LD} and F_{QD} do not contribute in massless approximation).

5.1 Flags of eeffLib

Here we give a very brief description of flags (user options) of eeffLib. While creating the code, we followed the principle to preserve as much as possible the meaning of flags as described in the ZFITTER description [6]. In the list below, a comment 'as in ZFD' means that the flag has exactly the same meaning as in [6].

- `ALEM=3  ! as in ZFD`
- `ALE2=3  ! as in ZFD`
- `VPOL=0  ! =0 \alpha(0); =1,=2 as in ZFD; =3 is reserved for later use`
  Note that the flag is extended to VPOL=0 to allow calculations 'without running of α'.
- `QCDC=0  ! as in ZFD`
- `ITOP=1  ! as in DIZET (internal flag)`
- `GAMS=1  ! as in ZFD`
- `WEAK=1  ! as in ZFD (use WEAK=2 in v6.30 to throw away some HO-terms)`
- `IMOMS=1 ! =0 \alpha-scheme; =1 GFermi-scheme`
  New meaning of an old flag: switches between two renormalization schemes;

- `BOXD=0  ! =0` without any boxes
  `! =1` with $\gamma\gamma$ box
  `! =2` with $Z\gamma$ box
  `! =3` with $\gamma\gamma$ and $Z\gamma$ boxes; 1, 2, 3 are used together with `WEAK=0`
  `! =4` with WW box
  `! =5` with WW and ZZ boxes; 4, 5 are used together with `WEAK=1`
- `GAMZTR=1! =0 GAMZ=0; =1 GAMZ.NE.0`
  Treatment of Γ_Z. The option is implemented for the sake of comparison with `FeynArts`.
- `EWFFTR=0! =0 EWFFs ; =1 RHO-KAPPAS`
  Treatment of EW form factors; switches between form factors and effective `ZFITTER` couplings ρ and κ's. The option is implemented for comparison with `ZFITTER`.
- `FERMTR=1! =1 a 'standard' set of fermions masses; =2,3 'modified'`
  Treatment of fermionic masses; switches between three different sets of 'effective quark masses'.

Table 1: EWFF for the process $e^+e^- \to u\bar{u}$. `eeffLib`–`ZFITTER` comparison.

Without EW boxes				
Quantity		$E_{\rm cm}$		
$\sqrt{s}$		100 GeV	200 GeV	300 GeV
F_{LL}	$M_W/10$	$13.47777 - i1.84781$	$16.22034 - i10.49408$	$23.75241 - i11.27464$
	M_W	$13.47777 - i1.84781$	$16.22034 - i10.49408$	$23.75241 - i11.27464$
	$10M_W$	$13.47777 - i1.84781$	$16.22034 - i10.49408$	$23.75241 - i11.27464$
`ZFITTER`		$13.47771 - i1.84786$	$16.22031 - i10.49405$	$23.75237 - i11.27464$
F_{QL}	$M_W/10$	$29.34725 + i3.67334$	$30.33892 + i3.34535$	$31.64554 + i2.75260$
	M_W	$29.34725 + i3.67334$	$30.33891 + i3.34535$	$31.64554 + i2.75260$
	$10M_W$	$29.34725 + i3.67334$	$30.33891 + i3.34535$	$31.64554 + i2.75260$
`ZFITTER`		$29.34720 + i3.67330$	$30.33889 + i3.34535$	$31.64552 + i2.75259$
F_{LQ}	$M_W/10$	$29.13302 + i3.26972$	$30.03854 + i1.54158$	$31.68636 - i0.22635$
	M_W	$29.13302 + i3.26972$	$30.03854 + i1.54158$	$31.68636 - i0.22635$
	$10M_W$	$29.13302 + i3.26972$	$30.03854 + i1.54158$	$31.68636 - i0.22635$
`ZFITTER`		$29.13304 + i3.26973$	$30.03855 + i1.54163$	$31.68635 - i0.22634$
F_{QQ}	$M_W/10$	$44.90390 + i8.85688$	$43.80287 + i10.02412$	$44.21224 + i10.83899$
	M_W	$44.90389 + i8.85688$	$43.80285 + i10.02412$	$44.21222 + i10.83899$
	$10M_W$	$44.90390 + i8.85688$	$43.80286 + i10.02412$	$44.21223 + i10.83899$
`ZFITTER`		$44.90392 + i8.85688$	$43.80285 + i10.02411$	$44.21224 + i10.83894$
WW is added				
F_{LL}	$M_W/10$	$12.94471 - i1.84781$	$9.34003 - i9.42493$	$9.03774 - i11.56004$
	M_W	$12.94471 - i1.84781$	$9.34003 - i9.42493$	$9.03774 - i11.56004$
	$10M_W$	$12.94471 - i1.84781$	$9.34003 - i9.42493$	$9.03774 - i11.56004$
`ZFITTER`		$12.94468 - i1.84786$	$9.34065 - i9.42467$	$9.03903 - i11.55958$

Table 2: EWFF for the process $e^+e^- \to u\bar{u}$. eeffLib–ZFITTER comparison.

With ZZ boxes				
Quantity		$E_{\rm cm}$		
$\sqrt{s}$		100 GeV	200 GeV	300 GeV
F_{LL}	$M_W/10$	$12.89587 - i1.84781$	$8.24674 - i10.64677$	$8.98241 - i12.88512$
	M_W	$12.89586 - i1.84781$	$8.24673 - i10.64677$	$8.98241 - i12.88512$
	$10M_W$	$12.89587 - i1.84781$	$8.24673 - i10.64677$	$8.98241 - i12.88512$
ZFITTER		$12.89583 - i1.84786$	$8.24736 - i10.64651$	$8.98370 - i12.88466$
F_{QL}	$M_W/10$	$29.30451 + i3.67334$	$29.38219 + i2.27613$	$31.59712 + i1.59304$
	M_W	$29.30451 + i3.67334$	$29.38218 + i2.27613$	$31.59712 + i1.59304$
	$10M_W$	$29.30451 + i3.67334$	$29.38219 + i2.27613$	$31.59712 + i1.59304$
ZFITTER		$29.30445 + i3.67330$	$29.38216 + i2.27613$	$31.59710 + i1.59304$
F_{LQ}	$M_W/10$	$29.10829 + i3.26972$	$29.48510 + i0.92306$	$31.65836 - i0.89713$
	M_W	$29.10829 + i3.26972$	$29.48509 + i0.92306$	$31.65835 - i0.89713$
	$10M_W$	$29.10829 + i3.26972$	$29.48509 + i0.92306$	$31.65835 - i0.89713$
ZFITTER		$29.10832 + i3.26973$	$29.48512 + i0.92312$	$31.65835 - i0.89711$
F_{QQ}	$M_W/10$	$44.88226 + i8.85688$	$43.31856 + i9.48287$	$44.18773 + i10.25200$
	M_W	$44.88226 + i8.85688$	$43.31854 + i9.48287$	$44.18771 + i10.25200$
	$10M_W$	$44.88226 + i8.85688$	$43.31855 + i9.48287$	$44.18772 + i10.25200$
ZFITTER		$44.88228 + i8.85688$	$43.31854 + i9.48286$	$44.18773 + i10.25196$

5.2 eeffLib–ZFITTER comparison of scalar form factors

First of all we discuss the results of a computation of the four scalar form factors,

$$F_{LL}(s,t), \quad F_{QL}(s,t), \quad F_{LQ}(s,t), \quad F_{QQ}(s,t), \tag{5.123}$$

for three variants:
1) without EW boxes, i.e. without gauge-invariant contribution of ZZ boxes, and without $\xi = 1$ part of the WW box, Eq. (2.93);
2) without ZZ boxes;
3) with full content of EWRC.

In this comparison we use flags as in subsection 5.1 and, moreover,

$$\begin{aligned} M_W &= 80.4514958 \text{ GeV}, \\ \Delta r &= 0.0284190602\,, \\ \Gamma_Z &= 2.499776 \text{ GeV}. \end{aligned} \tag{5.124}$$

In Table 1 we show an example of comparison of four form factors $F_{LL,QL,LQ,QQ}(s,t)$ between the eeffLib, where we set $m_t = 0.2$ GeV and ZFITTER (the latter is able to deliver only massless results). The form factors are shown as complex numbers for the three c.m.s. energies (for $t = m_t^2 - s/2$) and for the three values of scale $\mu = M_W/10,\ M_W,\ 10M_W$. The table demonstrates scale independence and very good agreement with `ZFITTER` results (6 or 7 digits). One should stress that total agreement with `ZFITTER` is not expected because in the `eeffLib` code we use massive expressions to compute the nearly massless case. Certain numerical cancellations leading to losing some numerical precision are expected. We should conclude that the agreement is very good and uniquely demonstrates that our formulae have the correct $m_t \to 0$ limit.

In Table 2 we show a similar comparison with `ZFITTER` when ZZ boxes are added. As seen, the agreement has not deteriorated.

5.3 `eeffLib`–`ZFITTER` comparison of IBA cross-section

As the next step of the comparison of `eeffLib` with calculations from the literature, we present a comparison of the IBA cross-section.

In Table 3 we show the differential cross-section Eq. (4.121) in pb for three values of $\cos\vartheta = -0.9,\ 0,\ +0.9$, with IPS of Eq. (5.124) and without running e.m. coupling, i.e. $\alpha(s) \to \alpha$.

Table 3: IBA, First row – `ZFITTER` ($u\bar{u}$ channel); second row – `eeffLib` ($m_t = 0.1$ GeV); third row – `eeffLib` ($m_t = 173.8$ GeV).

$\sqrt{s}$	$100GeV$	$200GeV$	$300GeV$	$400GeV$	$700GeV$	$1000GeV$
	47.664652	0.291823	0.169510			
$\cos\vartheta = -0.9$	47.661401	0.291827	0.169515	0.103284	0.035318	0.017203
				0.162579	0.043974	0.018850
	59.768387	1.718830	0.695061			
$\cos\vartheta = 0$	59.770715	1.718870	0.695072	0.376868	0.117276	0.055870
				0.264874	0.112923	0.054211
	168.981978	5.954048	2.292260			
$\cos\vartheta = 0.9$	168.991272	5.954166	2.292289	1.222343	0.372903	0.176030
				0.438952	0.293415	0.154784

Next, we present the same comparison as in Table 3, but now with running e.m. coupling. Since the flags setting `VPOL=1`, which is relevant to this case, affects `ZFITTER` numbers, we now use, instead of Eq. (5.124), the new `INPUT` set:

$$\begin{aligned} M_W &= 80.4467671\ \text{GeV}, \\ \Delta r &= 0.0284495385\,, \\ \Gamma_z &= 2.499538\ \text{GeV}. \end{aligned} \tag{5.125}$$

The numbers, collected in Table 4, exhibit good level of agreement.

Finally, in Table 5, we give a comparison of the cross-section integrated within the angular interval $|\cos\vartheta| \le 0.999$. (Flags setting is the same as for Table 4.)

Table 4: IBA, First row – ZFITTER ($u\bar{u}$ channel); second row – eeffLib ($m_t = 0.1$ GeV); third row – eeffLib ($m_t = 173.8$ GeV).

$\sqrt{s}$	$100GeV$	$200GeV$	$300GeV$	$400GeV$	$700GeV$	$1000GeV$
	45.404742	0.386966	0.225923			
$\cos\vartheta = -0.9$	45.404593	0.386966	0.225923	0.138065	0.048621	0.024155
				0.195069	0.057892	0.025877
	60.382423	1.882835	0.771939			
$\cos\vartheta = 0$	60.382553	1.882835	0.771938	0.421409	0.133474	0.064244
				0.303984	0.130208	0.062853
	173.467517	6.450000	2.510881			
$\cos\vartheta = 0.9$	173.467515	6.449995	2.510877	1.346616	0.417292	0.198839
				0.493006	0.330480	0.175598

Table 5: eeffLib–ZFITTER comparison of the total cross-section. Cross-sections are given in picobarns: the first row – $\sigma^{tf}_{\rm tot}$, i.e. eeffLib ($m_t = 0.1$ GeV); the second row – $\sigma^{ZF}_{\rm tot}$, i.e. ZFITTER ($u\bar{u}$ channel); the last entry shows the deviation $\left(\sigma^{tf}_{\rm tot} - \sigma^{ZF}_{\rm tot}\right)/\sigma^{ZF}_{\rm tot}$ in per mill.

100 GeV		200 GeV		300 GeV	
$\sigma_{\rm tot}$	$\sigma_{\rm FB}$	$\sigma_{\rm tot}$	$\sigma_{\rm FB}$	$\sigma_{\rm tot}$	$\sigma_{\rm FB}$
160.8981	70.98419	5.021797	3.360836	2.031750	1.269552
160.8980	70.98406	5.021808	3.360848	2.031754	1.269556
+0.001	+0.002	-0.002	-0.004	-0.002	-0.003

A typical deviation between eeffLib and ZFITTER is of the order $\sim 10^{-6}$, i.e. of the order of the required precision of the numerical integration over $\cos\vartheta$. Examples of numbers obtained with eeffLib, which were shown in this section, demonstrate that ZFITTER numbers are recovered for light m_t.

We conclude this subsection with a comment about technical precision of our calculations (modulo bugs, of course). We do not use looptools package [23]. For all PV functions, but one, namely D_0 function, we use our own coding where we can control precision internally and, typically, we can guarantee 9-10 digits precision. For D_0 function we use, instead, REAL*8 TOPAZ0 coding [22] and the only accessible for us way to control the precision is to compare results with those computed with REAL*16 TOPAZ0 coding. This was done for a typical D_0 function entering WW box contribution. We got an agreement within 9 digits between these two versions for all $\sqrt{s} = 400,\ 700,\ 1000$ GeV and $\cos\theta = 0.9,\ 0,\ -0.9$.

5.4 About a comparison with the other codes

As is well known, the one-loop differential cross-section of $e^+e^- \to t\bar{t}$ may be generated with the aid of the FeynArts system [23]. FeynArts-generated versions of the code with and without

QED contributions are available [24], and an attempt to compare results was undertaken. We compared $d\sigma/d\cos\theta$ without QED contributions at $\sqrt{s}=400,700,1000$ GeV and three values of $\cos\theta=0.9,\ ,0,\ -0.9$. An agreement of numbers for the Born cross-section within 6 digits was found, while for the one-loop corrected cross-section we managed to reach an agreement within $1-3\%$ only.

There is another FORTRAN code for $t\bar{t}$ production. It was originally written for the MSSM [25], but it has also been tailored for the SM. So far we managed to completely agree with this code only for the Born cross-section; while we turned to the one-loop one, we realized that no separation between QED and EW corrections is implemented into this code. On the contrary, in the eeffLib version used to produce numbers for this paper, we coded only the EW part of the cross-section. A present, the QED part is also available in our code [17]. Moreover, this code produces cross-section integrated over the angle, while it would be more informative to compare the differential quantity:

$$\delta(\sqrt{s},\cos\vartheta)=\frac{d\sigma^{(1)}(s,t)/dt}{d\sigma^{(0)}(s)/dt}-1. \tag{5.126}$$

For the time being we limit ourselves by presenting eeffLib results for $\delta(\sqrt{s},\cos\vartheta)$ of Eq. (5.126), which are shown in Fig. 13. (Flags setting is the same as for Table 3.)

Furthermore, in Fig. 3 of paper [16], an interesting result is presented. We tried to reproduce it with the aid of eeffLib. The results are shown in Fig. 14. As might be seen from a comparison of two figures, there is nearly ideal agreement for $\sqrt{s}$ in the interval [500–3000] GeV, while above 3000 GeV the eeffLib curve goes a bit higher than the curve shown in [16]. Note, that both curves show a very similar M_H dependence. It is difficult to expect more from such a pilot comparison, because even input parameters and various options were not tuned.

Meantime, a Bielefeld–Zeuthen team [26] started alternative calculations using the DIANA system [27]. A comparison of results was undertaken. It showed good agreement of numbers.

Recently, we were provided with the numbers computed with the FeynArts system [28] for $d\sigma/d\cos\theta$ without QED contributions; they showed better agreement than we managed to reach ourselves.

The results of latest comparisons will be presented in more detail elsewhere.

Acknowledgements

We would like to thank our colleagues P. Christova and A. Andonov for fruitful discussions. We are indebted to W. Hollik and C. Schappacher for a discussion of issues of the comparison with FeynArts. We acknowledge a common work on numerical comparison with J. Fleischer, A. Leike, T. Riemann, and A. Werthenbach which helped us to debug our code. We are grateful to T. Riemann for a critical reading of selected sections of this text and useful comments. We also wish to thank G. Altarelli for extending to us the hospitality of the CERN TH Division at various stages of this work.

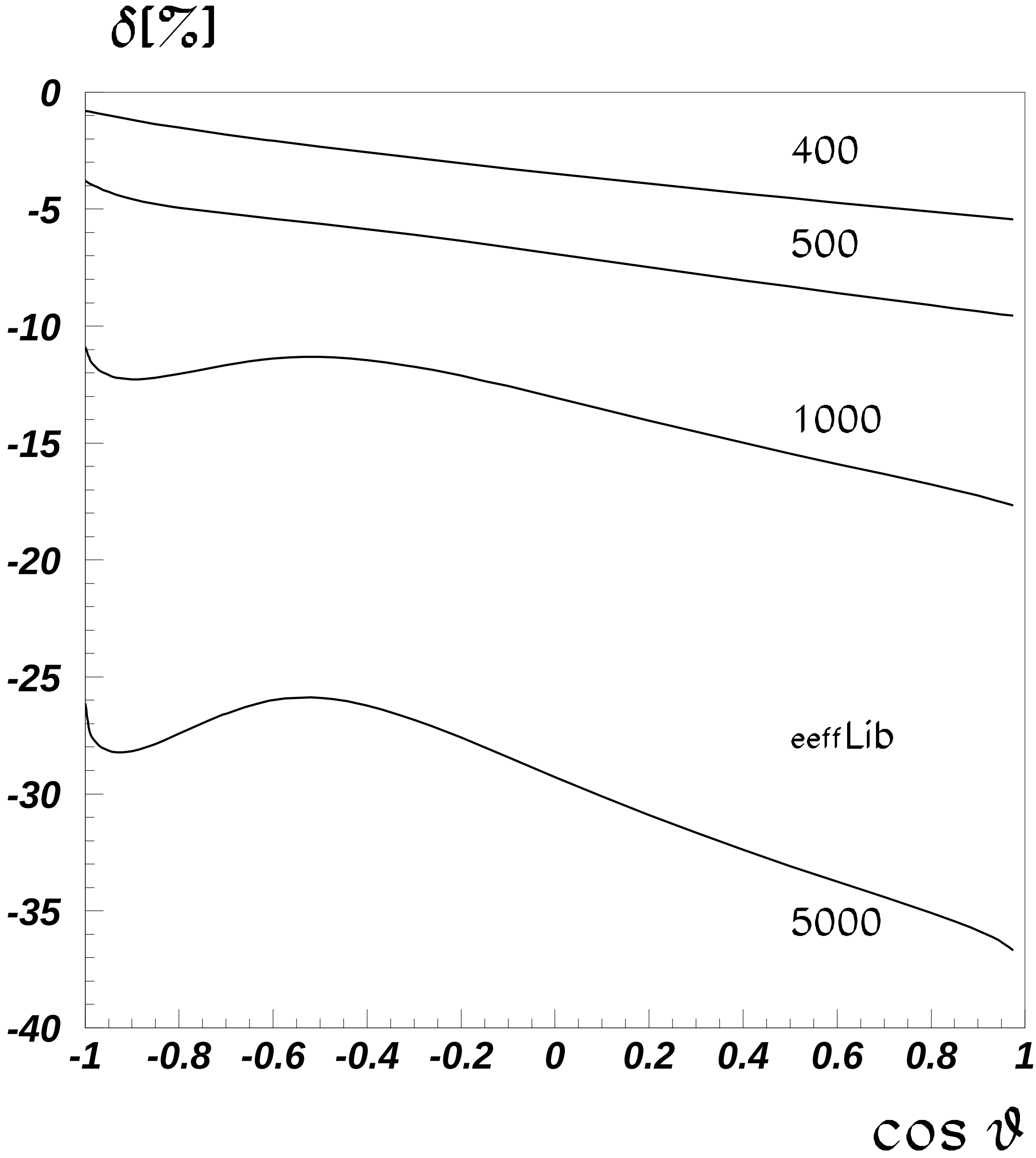

Figure 13: Relative EWRC δ [Eq. (5.126)] to the $e^+e^- \to t\bar{t}$ differential cross-section. Numbers near the curves show $\sqrt{s}$ in GeV.

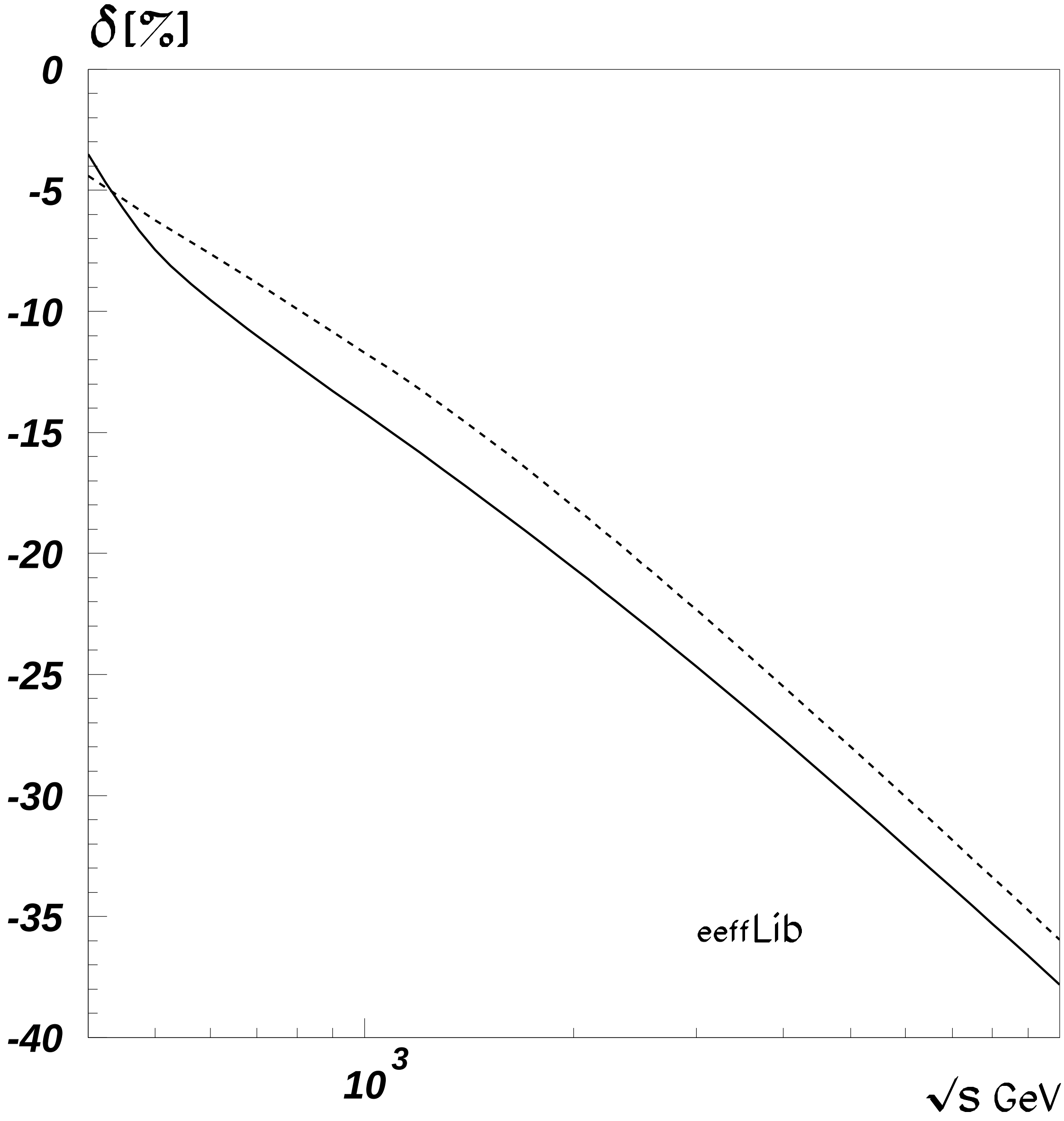

Figure 14: Relative EWRC to $e^+e^- \to t\bar{t}$ for $M_H = 100$ GeV (solid line) and $M_H = 1000$ GeV (dashed line).

References

[1] M. Beneke *et al.*,'Top quark physics', in *Proc. of the Workshop on Standard Model Physics (and More) at the LHC*, CERN 2000–004 (G. Altarelli and M. Mangano, eds.), pp. 419–529, 2000.

[2] F. Piccinini, *Nucl. Phys. Proc. Suppl.* **89** (2000) 31.

[3] A. Denner, S. Dittmaier, M. Roth, and D. Wackeroth, *Nucl. Phys.* **B587** (2000) 67–117.

[4] M. L. Nekrasov, *Eur. Phys. J.* **C19** (2001) 441–454.

[5] G. Passarino, D. Bardin, L. Kalinovskaya, P. Christova, G. Nanava, A. Andonov, and S. Bondarenko, contributors to `CalcPHEP`.

[6] D. Bardin, M. Bilenky, P. Christova, M. Jack, L. Kalinovskaya, A. Olchevski, S. Riemann, and T. Riemann, 'ZFITTER v.6.21: A semi-analytical program for fermion pair production in e^+e^- annihilation', DESY–Zeuthen preprint 99-070 (1999), `hep-ph/9908433`, *Comput. Phys. Commun.*, **133** (2001) 229–395.

[7] D. Bardin and G. Passarino, 'The standard model in the making: Precision study of the electroweak interactions', Oxford, UK: Clarendon, 1999.

[8] J. Fleischer and F. Jegerlehner, *Phys. Rev.* **D23** (1981) 2001–2026.

[9] F. Jegerlehner, Talk presented at Topical Conf. on Radiative Corrections in $SU(2)_L \otimes U(1)$, Trieste, Italy, 1983.

[10] F. Jegerlehner and J. Fleischer, *Phys. Lett.* **B151** (1985) 65–68.

[11] F. Jegerlehner and J. Fleischer, *Acta Phys. Polon.* **B17** (1986) 709.

[12] J. Fleischer, F. Jegerlehner, and M. Zralek, Presented at 11th Int. School of Theoretical Physics, Testing the Standard Model, Szczyrk, Poland, 1987.

[13] W. Beenakker, S. C. van der Marck, and W. Hollik, *Nucl. Phys.* **B365** (1991) 24–78.

[14] W. Beenakker and W. Hollik, *Phys. Lett.* **B269** (1991) 425–431.

[15] W. Beenakker, A. Denner, and A. Kraft, *Nucl. Phys.* **B410** (1993) 219–244.

[16] V. Driesen, W. Hollik, and A. Kraft, 'Top pair production in e^+e^- collisions with virtual and real electroweak radiative corrections', Karlsruhe University preprint (1996), `hep-ph/9603398`.

[17] A. Andonov, D. Bardin, S. Bondarenko, P. Christova, L. Kalinovskaya, and G. Nanava, 'Further study of the $e^+e^- \to t\bar{t}$ process with the aid of `CalcPHEP` system', in preparation.

[18] D. Bardin, L. Kalinovskaya, and G. Nanava, `FORTRAN` code `eeffLib`, December 2000.

[19] D. Bardin, M. Bilenky, P. Christova, M. Jack, L. Kalinovskaya, A. Olchevski, S. Riemann, and T. Riemann, ZFITTER v.6.30, obtainable from `http://www.ifh.de/~riemann/` and from `/afs/cern.ch/user/b/bardindy/public`.

[20] J. Vermaseren, 'New features of FORM', preprint NIKHEF-00-032 (2000), `math-ph/0010025`.

[21] G. Passarino, *Nucl. Phys.* **B361** (1991) 351–391.

[22] G. Montagna, O. Nicrosini, F. Piccinini and G. Passarino, *Comput. Phys. Commun.* **117** (1999) 278.

[23] J. Küblbeck, M. Böhm, A. Denner, *Comput. Phys. Commun.* **60** (1990) 165; T. Hahn, M. Perez-Victoria, *Comput. Phys. Commun.* **118** (1999) 153; T. Hahn, *Nucl. Phys. Proc. Suppl.* **89** (2000) 231; T. Hahn, *Comput. Phys. Commun.* **140** (2001) 418; T. Hahn, C. Schappacher, `hep-ph/0105349`.

[24] The code was taken from `http://www.hep-processes.de`. (Courtesy W. Hollik.)

[25] W. Hollik and C. Schappacher, *Nucl. Phys.* **B545** (1999) 98–140.

[26] J. Fleischer, T. Riemann, and A. Werthenbach, private communication.

[27] J. Fleischer and M. Tentyukov, 'A Feynman Diagram Analyser DIANA' - Graphic Facilities, Contribution to the Proceedings of 7th International Workshop on Advanced Computing and Analysis Techniques in Physics Research (ACAT 2000), Batavia, Illinois, 2000, `hep-ph/0012189`.

[28] The numbers for the comparison were provided by C. Schappacher.